UC Irvine

UC Irvine Electronic Theses and Dissertations

Title

Electrochemical Evaluation of Bipolar Ion-Exchange Membranes for Solar Fuels

Permalink

https://escholarship.org/uc/item/3pc416c6

Author

Reiter, Ronald

Publication Date

2015

Peer reviewed|Thesis/dissertation

eScholarship.org Powered by the California Digital Library
University of California

UNIVERSITY OF CALIFORNIA,
IRVINE

Electrochemical Evaluation of Bipolar Ion-Exchange Membranes for Solar Fuels

THESIS

submitted in partial satisfaction of the requirements
for the degree of

MASTER OF SCIENCE

in Chemistry

by

Ronald Stephen Reiter

Thesis Committee:
Assistant Professor Shane Ardo, Chair
Associate Professor Matthew Law
Professor Reginald M. Penner

2015

Figure 1.3 © 2014 Wiley-VCH Verlag GmbH & Co. KGaA, Weinheim
All other materials © 2015 Ronald Stephen Reiter

DEDICATION

This thesis is dedicated to:

My parents, Tim and Sharon, for their unwavering support in all my endeavors.

My brother, Brenton, for all the good times that we have spent together.

My girlfriend, Rhianna, for supporting me day and night through the best and worst of times.

To my uncles and cousins for always asking, “What are you going to do next?” and pushing me to excel.

My friends, for our many game nights to keep my mind off school.

TABLE OF CONTENTS

	Page
LIST OF FIGURES	iv
ACKNOWLEDGMENTS	vi
ABSTRACT	vii
OVERVIEW	1
References	4
CHAPTER 1: Electrolyte Effects on the Electrochemistry of Bipolar Membranes	5
Introduction	5
Experimental	8
Results	11
Discussion	19
Conclusions	22
References	24
CHAPTER 2: Dye-Sensitized Ion-Exchange Membranes as Light-Driven Ion Pumps	25
Introduction	25
Experimental	27
Results	34
Discussion	39
Conclusions	43
References	43
APPENDIX A: Mathematica Code for Calculation of Laser Beam Diameter	44

LIST OF FIGURES

		Page
Figure 1.1	Commercial Anion and Cation Exchange Membranes	6
Figure 1.2	Electrochemical Cell Diagram	11
Figure 1.3	Mobile Ion Movement in BPM During Forward and Reverse Polarization	11
Figure 1.4	*J–E* Behavior of BPM in 1 M NaCl	12
Figure 1.5	*J–E* Behavior of BPM in 1 M HCl/NaOH	13
Figure 1.6	Membrane Potential of BPM in 1 M HCl/NaOH with H_2 Sparging	14
Figure 1.7	*J–E* Behavior of BPM in 0.01 M HCl/NaOH	15
Figure 1.8	*J–E* Behavior of BPM in 1 M HCl/KCl and 1 M KCl/NaOH	16
Figure 1.9	*J–E* Behavior of BPM in 0.01 M HCl/NaOH + 1 M NaCl or KCl	17
Figure 1.10	Membrane Potential of BPM versus NaCl Concentration	18
Figure 1.11	Membrane Potential of BPM in 0.01 M HCl/NaOH + 0.2 or 0.1 M KCl	19
Figure 2.1	Final Step in Nafion Synthesis	26
Figure 2.2	Molecular Structure of CS3 Photoacid	27
Figure 2.3	Nafion Precursor Functionalization Reaction with CS3 Photoacid	28
Figure 2.4	Molecular Structure of Ionic Dyes	29
Figure 2.5	Digital Photograph of Nafion-CS3 Membranes	34
Figure 2.6	Digital Photograph of Nafion Membranes Soaked in Ionic Dyes	35
Figure 2.7	UV–Vis Spectra of Nafion–CS3 Membranes Soaked in Ionic Dyes	36
Figure 2.8	UV–Vis Spectra of Nafion Soaked in Ionic Dyes	36
Figure 2.9	FTIR %T Spectra of Nafion Membranes	37
Figure 2.10	Digital Photograph of Nafion–CS3 Membrane Fluorescing	38
Figure 2.11	Membrane Potential of Nafion–CS3 Membrane Under Laser Illumination	38

Figure 2.12 *J–E* Behavior of Nafion–CS3 BPM Under Illumination 39

ACKNOWLEDGMENTS

I would like to thank to my committee chair, Professor Shane Ardo for his guidance; without him, this thesis would not have been possible.

I would like to thank the past and current members of the Ardo Group for their support and help with experiments.

Finally, I would like to thank the staff members in the chemistry graduate division for their guidance and assistance during my graduate studies at UCI.

Figure 1.3 was reproduced with permission from Scheme 1 in *Assessing the Utility of Bipolar Membranes for use in Photoelectrochemial Water-Splitting Cells*, written by Vargas-Barbosa et al., published in ChemSusChem by Wiley-VCH on behalf of ChemPubSoc Europe.

This research was funded in part by the UCI Chancellor's Fellowship.

ABSTRACT

Electrochemical evaluation of bipolar ion-exchange membranes for solar fuels

By

Ronald Stephen Reiter

Master of Science in Chemistry

University of California, Irvine, 2015

Assistant Professor Shane Ardo, Chair

Photoelectrochemical cells that utilize bipolar ion-exchange membranes (BPMs) can support and maintain a pH difference across the membrane. Redox-inactive salts are often also incorporated in these cells and it is unclear if salts have an effect on the electrostatics within the cell and perceived thermodynamics of the overall redox chemistry. In this thesis, commercial BPMs wetted by various electrolytes were investigated, e.g. in the presence of acid, base, and/or salt. The electrochemical behavior of the BPMs was assessed by measuring the current density *vs* potential behavior. The results suggest that potential differences measured across BPMs may not always reflect the pH of the bulk electrolyte and therefore may require additional information in order to justify the overall free energy required for the redox reactions.

The second half of this thesis was dedicated to the development of an artificial light-driven ion pump using BPM materials. An activated Nafion precursor membrane was functionalized with newly developed photoacid molecules and sandwiched between an anion-exchange membrane and a cation-exchange membrane. The photoelectrochemical properties of the resulting photoacid-functionalized BPM were measured and a photovoltaic response was observed. These initial findings provide a solid foundation for future research into customized BPMs to be used as artificial light-driven ion pumps.

Overview

In 2012, humans consumed > 17.5 TW of power.[1] The sun is the only entirely renewable, clean, and safe source of energy that can provide this power and power our planet in a sustainable manner.[2] Although photovoltaics are very efficient at converting photon energy into usable electricity and are becoming cost-competitive with other means of generating electricity,[3] their wide-spread adoption is limited by their inability to store transient photon energy for use at night and in regions that do not have much direct sunlight.[4] One of the simplest chemical transformations that could store this electricity using an abundant electron source is water electrolysis (i.e. "water splitting"). Therefore, inexpensive solar water splitting has been termed a Holy Grail of energy science.[5]

Solar water splitting technologies require that solar photons are not only harvested but that their energy is used to perform electrochemical reactions at their surfaces, notably oxidation of water to oxygen (i.e. the oxygen-evolution reaction (OER)) and reduction of water to hydrogen (i.e. the hydrogen-evolution reaction (HER)), all while separating the O_2 and H_2 reaction products to circumvent generation of an explosive mixture of H_2 and O_2, and generating a pure stream of H_2 for ultimate use.[6] The materials challenge, and Holy Grail, for such a design is to identify a single, inexpensive material that can perform all desired processes; however, no such material has been identified. Instead several membrane-separated light-absorbing semiconductors are often arranged electrically and optically in series and coated with thin layers of efficient electrocatalysts that do not greatly attenuate sunlight transmission but also are able to drive the desired electrochemical reactions at large efficiencies and with small catalytic overpotentials. Unfortunately, no sets of at least five materials (i.e. light absorbers, electrocatalysts, and membranes) that are stable in one electrolyte condition have been identified.

While recent research has advanced the use of thin protective coatings to stabilize inherently thermodynamically unstable semiconductors from corrosion and passivation in many electrolytes,[7] no electrocatalysts for the OER exist that are stable in acid, where only IrO_2 and RuO_2 are state-of-the-art.[8] In base, a combination of a NiMo alloy HER electrocatalyst and FeNi(O)OH OER electrocatalyst are suitable choices, but no ion-exchange membranes are chemically and mechanically stable, highly permselective, and ionically conductive in alkaline conditions.[9] Therefore, it is of great research interest to develop systems that are stable in a single electrolyte over extended periods of time, while also being efficient and inexpensive (i.e. consisting of earth-abundant elements and/or requiring mature or low-energy fabrication processes). Toward this, recently bipolar ion-exchange membranes (BPMs) have been used in demonstrations of solar water splitting because they can relax these requirements by allowing sustainable pH differences (i.e. two different pH electrolytes) to be used.[10] Bipolar membranes consist of a permselective cation-exchange membrane (CEM) layer laminated to a permselective anion-exchange membrane (AEM) layer.[11] Under conditions of strong reverse-bias polarization they dissociate water at their interface and transport protons and hydroxide ions through the CEM layer and AEM layer, respectively, which neutralize protons and hydroxide ions liberated by the water splitting reactions. Therefore, at steady-state BPMs allow the original pH values to be maintained, even during active water splitting. However, few studies on BPMs have been conducted under conditions where potential drop due to ion migration (i.e. *iR* drop) and local pH differences are quickly neutralized (i.e. separating strong acid and strong base).[12,13] We set-out to examine the properties of BPMs under these conditions and in the presence of varying amounts of salt, which are most likely those that will be used in efficient solar fuels devices.

It is also proposed that BPMs which separate acidic and alkaline electrolytes form an internal electric field and built-in potential at the interface of their CEM layer and AEM layer.[14] This electric field arises from equilibration of protons and hydroxide ions in this interfacial region, where the magnitude and size of this electric field can be calculated using Poisson's equation.[15] The mechanism and driving force for formation of this depletion region in BPMs is very similar to that in semiconductor pn-junctions, and because materials with pn-junctions form the most efficient photovoltaics we therefore wondered whether BPMs could function as light-driven ion pumps, converting sunlight energy into ionic power. Toward this, we sensitized BPMs to sunlight absorption through covalent attachment of photoacid molecules to ion-exchange membranes and evaluated their photoelectrochemical and photophysical properties. The hypothesis was that upon absorption of light, the energy in the photons would be converted into a change in chemical potential of protons such that optical excitation resulted in net ionic power generation, i.e. a photocurrent and photovoltage.

The conditions under which BPMs were studied in this research are relevant to solar fuels technologies. Results from these studies will help identify conditions where solar fuels devices can operate that are more suitable for prolonged and sustained use of many efficient and inexpensive electrocatalysts. Moreover, through better understanding of the sensitization cycle of photoacid-functionalized ion-exchange membranes, additional power can be generated by the membrane to assist in the solar water-splitting chemistries. Collectively, this suite of results will help to identify avenues for continued and advanced research and development with the aims of lessening the output power requirements from the illuminated semiconductor light absorbers and ultimately realizing efficient, stable, and scalable solar fuels technologies.

References

(1) International Energy Statistics - EIA http://www.eia.gov/cfapps/ipdbproject/IEDIndex3.cfm?tid=44&pid=44&aid=2 (accessed Sep 2, 2015).

(2) Lewis, N. S.; Nocera, D. G. *Proc. Natl. Acad. Sci. U. S. A.* **2006**, *103*, 15729.

(3) Feldman, D.; Barbose, G.; James, T.; Weaver, S.; Fu, R.; Davidson, C. Photovoltaic System Pricing Trends 2014 Edition http://www.nrel.gov/docs/fy14osti/62558.pdf.

(4) Branz, H. Beyond Grid Parity: Spectrum-Efficient Solar Energy for Dispatchable Electricity or Dense Fuels http://www.arpa-e.energy.gov/sites/default/files/documents/files/SolarBeyondGridParity_Branz.pdf (accessed Sep 2, 2015).

(5) Bard, A.; Fox, M. A. *Acc. Chem. Res.* **1995**, *28*, 141.

(6) McKone, J. R.; Lewis, N. S.; Gray, H. B. *Chem. Mater.* **2014**, *26*, 407.

(7) Hu, S.; Shaner, M. R.; Beardslee, J. a; Lichterman, M.; Brunschwig, B. S.; Lewis, N. S. *Science* **2014**, *344*, 1005.

(8) McCrory, C. C. L.; Jung, S.; Ferrer, I. M.; Chatman, S.; Peters, J. C.; Jaramillo, T. F. *J. Am. Chem. Soc.* **2015**, *137*, 4347.

(9) Varcoe, J. R.; Atanassov, P.; Dekel, D. R.; Herring, A. M.; Hickner, M. a.; Kohl, P. a.; Kucernak, A. R.; Mustain, W. E.; Nijmeijer, K.; Scott, K.; Xu, T.; Zhuang, L. *Energy Environ. Sci.* **2014**, *7*, 3135.

(10) Ünlü, M.; Zhou, J.; Kohl, P. a. *J. Phys. Chem. C* **2009**, *113*, 11416.

(11) Simons, R.; Khanarian, G. *J. Membr. Biol* **1976**, *38*, 11.

(12) McDonald, M. B.; Ardo, S.; Lewis, N. S.; Freund, M. S. *ChemSusChem* **2014**, *7*, 3021.

(13) Vargas-Barbosa, N. M.; Geise, G. M.; Hickner, M. a.; Mallouk, T. E. *ChemSusChem* **2014**, *7*, 3017.

(14) Simons, R. *J. Memb. Sci.* **1993**, *78*, 13.

(15) Mafé, S.; Ramírez, P. *Acta Polym.* **1997**, *48*, 234.

Chapter 1: Electrolyte Effects on the Electrochemistry of Bipolar Membranes

Introduction

Ion-exchange membranes are used in most electrochemical technologies (e.g. fuel cells, electrolyzers, electrodialysis, chloralkali industry; not batteries)) to efficiently transport ions and to prevent mixing of chemical species between the electrolyte compartments on each side of the membrane. Typically, low-temperature (< 100 °C) ion-exchange membranes consist of a polymer material with an uncharged backbone and pendant fixed-charge functional groups. The permselectivity of these membranes arises from Donnan exclusion, where at thermal equilibrium there is a reduction in the concentration of mobile ions within the membrane due to a large concentration of fixed-charge groups of the same sign.[1,2] This generates an electric potential at the interface of the membrane, which is referred to as the Donnan potential. The Donnan potential and can be measured using reference electrodes that are sensitive to electric potential, and not the chemical potential of excluded species, such as the typical standard calomel electrode (SCE) or silver/silver–chloride (Ag/AgCl) electrode each connected to the main cell by a salt bridge.

Bipolar membranes (BPMs) are composed of two types of charged polymers. One layer is an anion-exchange membrane (AEM) layer (AEL), which contains of one of a variety of fixed cationic groups,[3,4] but typically quaternary ammonium functional groups, and results in permselective transport of anions. The second polymer is a cation-exchange membrane (CEM)

layer (CEL), which contains sulfonate functional groups to facilitate permselective transport of cations. The junction between the two ion-exchange layers is known as the space-charge region.

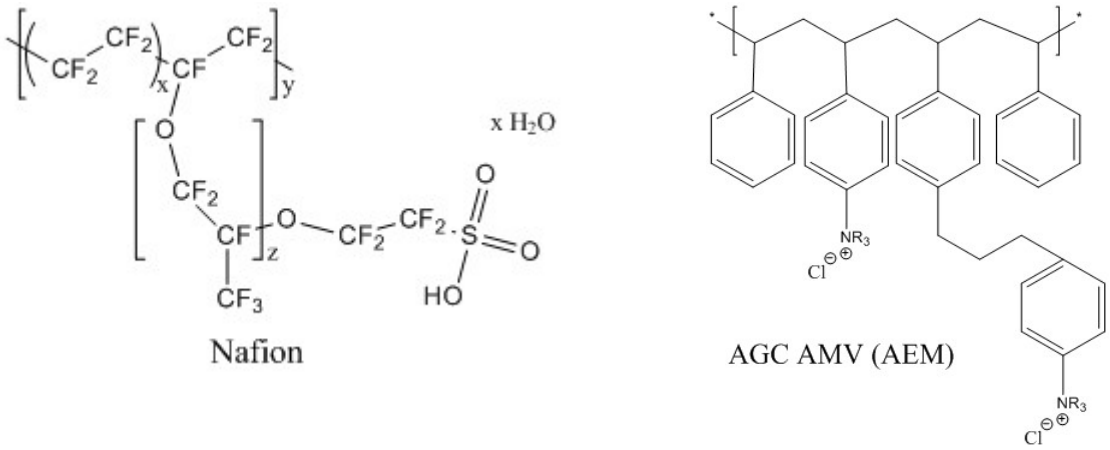

Figure 1.1. Commercially available ion exchange membranes. Nafion® (Left), a cation exchange membrane discovered by Walther Grot of DuPont and AMV (Right), an anion exchange membrane manufactured by AGC Engineering Co.

The current density *vs*. potential (*J–E*) behavior of these membranes is unique. In general, an AEM or CEM alone wetted by ~1 M electrolyte will exhibit a linear (ohmic) *J–E* response, because it acts as a layer that conducts only one type of ionic charge. However, a BPM rectifies current and its *J–E* response resembles that of a semiconductor diode. In addition, when a large enough reverse-bias polarization is applied to a BPM a breakdown condition can be achieved where water dissociation is rapidly facilitated at the AEM/CEM interface and the current increases by two orders-of-magnitude.

In 2009, Ünlü and Kohl showed that a BPM can be used as the solid electrolyte in a polymer-electrolyte-membrane fuel cell and therefore the two electrochemical half-reactions occurred in different pH environments.[5] The authors used a commercial BPM and drove H_2 oxidation at the strongly acidic CEM and O_2 reduction at the strongly alkaline AEM. The authors described that the initial difference in pH across the BPM did not change over time because each

ion that migrated to the interfacial region was replenished by proton-coupled electron-transfer reactions at the electrodes. Moreover, the thermodynamics for water formation (i.e. H_2 oxidation and O_2 reduction) did not constitute a potential savings or loss because the Nernstian potential response of the BPM was equal in magnitude but opposite in direction/sign to that of the redox reactions at the electrodes.

Follow-up work by Freund and colleagues and Mallouk and colleagues demonstrated that BPMs wetted by acid and base may also be useful in photoelectrochemical (electrolysis) applications, where the membranes are immersed in liquid electrolytes with pH values similar to those of the CEM or AEM which they contact.[6,7] In general, their results were in agreement with those of Ünlü and Kohl; however, use of a liquid electrolyte allowed the membrane potential drop to be measured selectively using typical electrochemical four-electrode techniques.[8] The most basic DC technique is analogous to solid-state four-point-probe measurements.[9] The results from the measurements with liquid electrolytes suggested that the BPM had a ~0.8 V potential drop across it and that the permselectivity of the layers precluded dark discharge of the pH difference. Many decades of data support that an electric potential drop at the interface of the CEM and AEM forms that opposes that of the difference in chemical potential of the protons and hydroxide ions,[10] analogous to the process that occurs in a semiconductor pn-junction upon initial equilibration between the doped regions, across the glass membrane of a pH probe, and at the interface of a single ion-exchange membrane that exhibits Donnan exclusion.[11–13]

Herein we carefully examine the *J–E* behavior of bipolar membranes wetted on one side by acidic aqueous electrolyte and on the other side by alkaline aqueous electrolyte, both in the absence and presence of extra supporting electrolyte. These conditions are relevant to devices for solar fuels generation and have not previously been reported in the peer-reviewed literature.

Experimental

Preparation of Bipolar Membranes

Fumatech FBM bipolar membrane was purchased from FuMA-Tech GmbH and stored in 1 M NaCl(*aq*). All pieces of FBM used for electrochemical measurements were cut fresh and immediately placed in an electrochemical cell and wetted by one or two electrolyte solution(s). The membrane was rinsed twice with the electrolyte solution to be used in the measurement and allowed to equilibrate for a period of 10 minutes after being wetted by the electrolyte solution(s) before performing the electrochemical measurements. For acid/base measurements, acid was used to rinse the CEM side of the cell and base was used on the AEM side of the cell. The electrolyte solutions were then drained a final time and new electrolyte was pipetted into the cell.

Preparation of the Electrochemical Cell

The electrochemical cell consisted of two Kel-F (poly(chlorotrifluoroethylene)) blocks each with pre-drilled holes for insertion of the electrodes and a central cylindrical channel for addition of the aqueous electrolyte solution (Figure 1.2). One side of the cell contained a quartz window. Platinum electrodes were fabricated by soldering a 1 cm long 300 μm diameter platinum wire to a piece of insulated tinned Cu wire and sealing the connection with Loctite Hysol 1C two-part epoxy. Unless noted otherwise, these were used as the power/current-carrying (working and counter) electrodes were placed on opposite sides of the membrane. The platinum electrodes were rinsed with deionized water after every electrochemical measurement and stored in dry conditions. Standard calomel electrodes (SCEs) were purchased from CH Instruments, Inc. and used as the reference electrodes, unless noted otherwise. The SCEs were removed from saturated KCl solutions, rinsed with deionized water, and placed in the electrochemical cell.

After each electrochemical measurement, the SCEs were rinsed with deionized water and placed in saturated KCl storage solutions. Reversible hydrogen electrodes (RHE) were platinum electrodes that were constructed identically to the ones mentioned above. H_2 gas was sparged into the electrochemical cell using 18-gauge needles placed in the third set of holes in the Kel-F blocks.

The electrochemical cell was connected to a BioLogic VSP-300 potentiostat. The current-carrying leads were attached to the platinum electrodes. The platinum electrode on the AEM side of the membrane served as the working electrode, while the platinum electrode on the CEM side of the membrane served as the counter electrode. The main two potential-sensing leads were attached to the SCEs on each side of the membrane so that the potential drop across the membrane could be probed. (In conventional three-electrode electrochemistry experiments, these two leads measure the potential between the working electrode and reference electrode.) A third (optional) potential-sensing lead was attached to the counter electrode to monitor its potential and help identify anomalous behavior.

Electrochemical Measurements of Bipolar Membranes

Before starting an electrochemical experiment, an open-circuit potential (E_{oc}) measurement was taken to ensure that the membrane had equilibrated with the electrolyte solutions. After verifying that the membrane potential was stable to within one millivolt for a period of 10 minutes, potentiostatic chronoamperometry measurements were performed. The *J–E* curve was constructed from a series of these potentiostatic chronoamperometry measurements, where the current at 300 seconds after the start of each potential step – when the value was independent of time – was plotted along with the corresponding potential applied at that step. In

order to ensure that the membrane was in good working condition for the entire *J–E* measurement, data points under reverse bias were obtained before those under forward bias where membrane delamination may occur due to excessive water formation at the AEM/CEM interface. Starting at the open-circuit condition, the potential was stepped in increments of +100 mV (50 mV increments from 650-950 mV) vs. E_{oc}; this constituted the reverse-bias portion of the *J–E* data where at which time the membrane potential was allowed to equilibrate back to its starting potential. Notably, in neutral-pH salt conditions E_{oc} was zero millivolts initially, and approximately 830 mV after the final reverse-bias chronoamperometry measurement. The forward-bias chronoamperometry data was obtained in the same manner as the reverse-bias data, except that the potential was stepped in increments of –100 mV.

Current densities were calculated by dividing the current passed through the cell by the geometric area of the membrane exposed to the aqueous electrolyte solution (1.54 cm^2). For all *J–E* data, a positive membrane potential corresponds to reverse-bias polarization, and a negative membrane potential corresponds to forward-bias polarization. During reverse-bias polarization, oxidation occurs at the working electrode, which is in contact with the electrolyte that wets the AEM, and reduction occurs at the counter electrode, which is in contact with the electrolyte that wets the CEM.

When evaluating open-circuit membrane potentials over time, the electrodes and extra electrode holes in the electrochemical cell were wrapped with Parafilm to seal off the electrolyte from air and attenuate pH changes due to carbon dioxide dissolution.

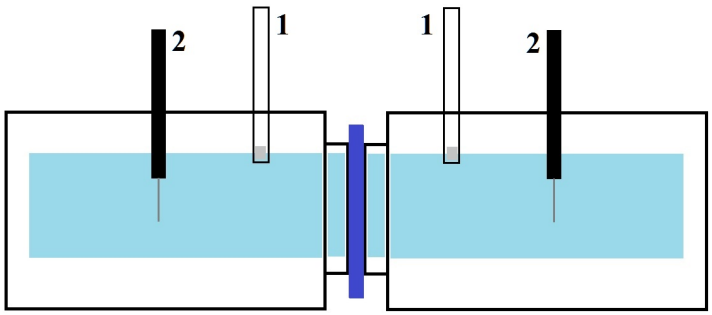

Figure 1.2. Schematic of the four-electrode setup used to evaluate the electrochemical behavior of a membrane (dark blue). Electrodes labeled (1) are nominally identical potential-sensing (reference) electrodes (SCE, Ag/AgCl wire, or RHE) and were used to measure the membrane potential. Electrodes labeled (2) are nominally identical current-carrying (working/counter) electrodes (Pt wire) and were used to pass current through the electrochemical cell.

Results

Bipolar membrane electrochemistry in aqueous salt solution

Figure 1.3 illustrates pathways of ionic migration during forward-bias and reverse-bias polarization of a BPM. Co-ion-leakage is a process where the ion-exchange layer transports mobile ions of the same charge type as the fixed charge groups within the membrane. The degree to which co-ion leakage occurs is dependent on the properties of the membrane and the concentration of salt;[14] ideally co-ion leakage occurs at a slow rate.

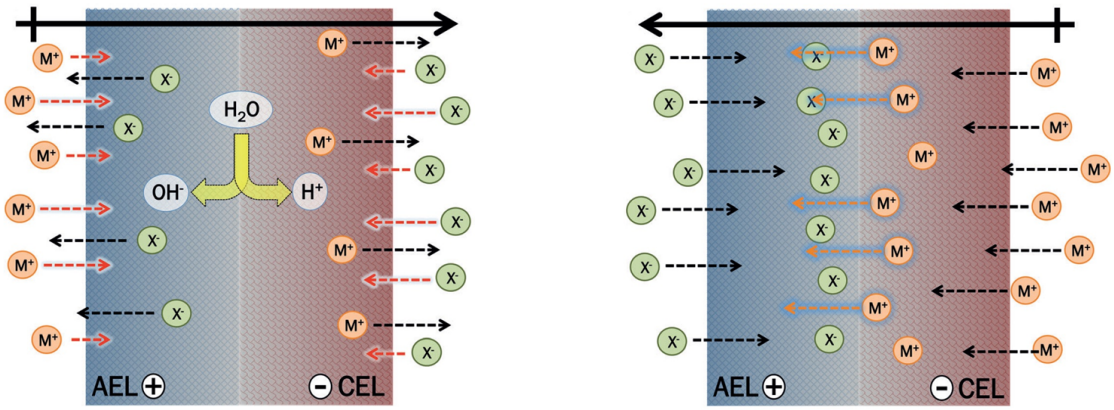

Figure 1.3.[7] Representation of movement of ions through a BPM. In reverse polarization (left), ions are removed from the space-charge region and water dissociation eventually occurs. In forward polarization (right), ions associate in the space-charge region. Black arrows show how the ions move through the appropriate ion exchange layer. Red arrows demonstrate co-ion leakage. Reproduced with permission from Scheme 1 in *Assessing the Utility of Bipolar Membranes for use in Photoelectrochemial Water-Splitting Cells*, written by Vargas-Barbosa et al.

The *J–E* behavior of a BPM wetted by 1 M NaCl(*aq*) is displayed in Figure 1.4. Based on membrane potentials between –1.0 V and +0.8 V it is clear that the BPM rectifies current. A device that rectifies current readily passes current when biased in one polarization direction (in this case, negative; forward-bias polarization) but does not pass a significant amount of current when biased in the opposite direction of polarization (in this case, positive; reverse-bias polarization). For reverse-bias membrane potentials in excess of ~830 mV, the current increased exponentially with applied potential due to water dissociation / breakdown.[2] Continued forward-bias polarization tended to degrade the BPM due to delamination of the two layers. This behavior has been attributed to ion transport from the bulk solution through the ion-exchange layers and into the interfacial space-charge region, where they recombine to form salt (Figure 1.3).[7]

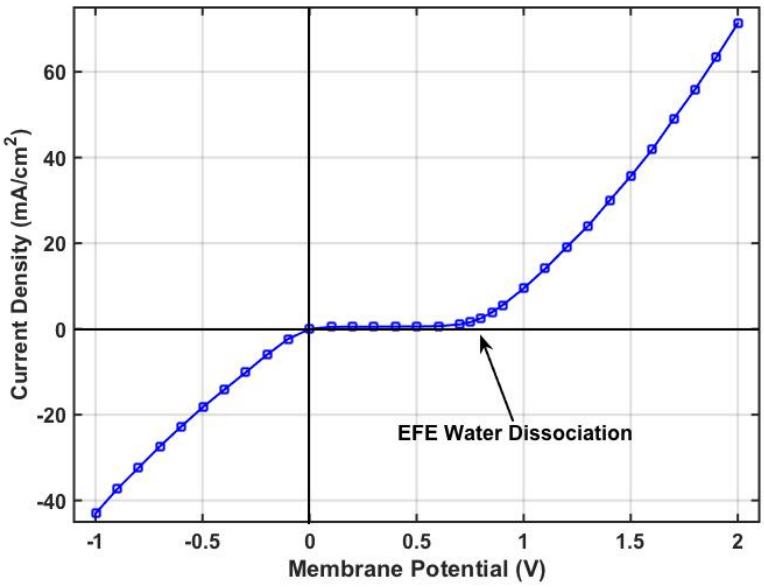

Figure 1.4. *J–E* behavior of a BPM wetted by 1 M NaCl(*aq*) (SCE | NaCl | CEM | AEM | NaCl | SCE) and recorded using SCE potential-sensing electrodes. Reverse (forward) bias polarization conditions occur at positive (negative) potentials.

Bipolar membrane electrochemistry when wetted by acid and base

Shown in Figure 1.5 is the *J–E* behavior of a BPM wetted by strong acid on one side and strong base on the other side (1 M HCl(*aq*)/NaOH(*aq*)). The membrane exhibited an open-circuit potential of ~0.8 V and displayed no region of limiting current when reverse biased (Figure 1.7, inset). Also, biasing the membrane several hundred millivolts positive or negative of the open-circuit potential resulted in a nearly ohmic response with significant current being passed in either bias direction.

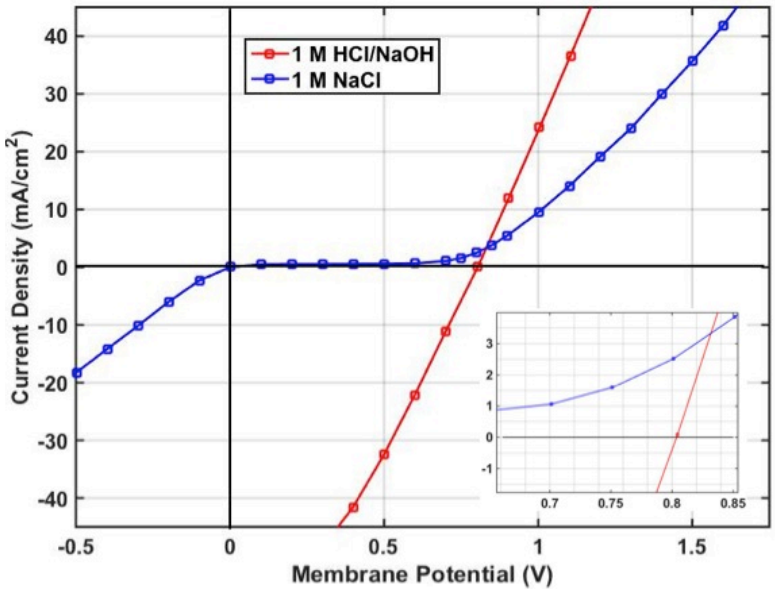

Figure 1.5. *J–E* behavior of a BPM wetted by 1 M NaCl(*aq*) (blue; same data as in Figure 1.4) (SCE | NaCl(*aq*) | CEM | AEM | NaCl(*aq*) | SCE) and wetted by 1 M HCl on the CEM side and 1 M NaOH(*aq*) on the AEM side (red; SCE | HCl(*aq*) | CEM | AEM | NaOH(*aq*) | SCE). Both data sets were recorded using SCE potential-sensing electrodes. The inset shows data with the same axes and at membrane potentials near 0.8 V.

While the membrane potential was ~0.8 V when measured using two SCEs and wetted by 1 M HCl(*aq*)/NaOH(*aq*), when the potential-sensing electrodes were replaced with quasi-reference electrodes (i.e. Pt in contact with the H_2/H^+ redox couple), the membrane potential was ~0 V (Figure 1.6).

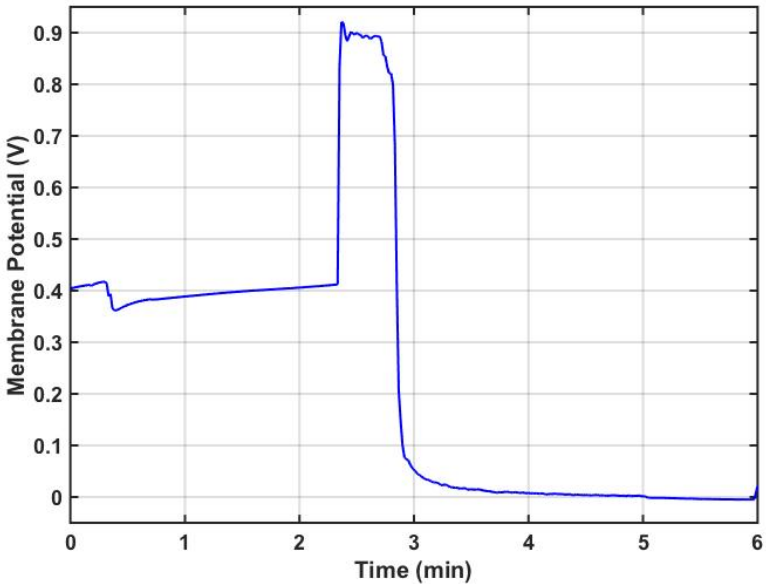

Figure 1.6. Potential across a BPM as a function of time while wetted by 1 M HCl(*aq*) on the CEM side and 1 M NaOH(*aq*) on the AEM side (Pt(*s*) | H_2(*g*) | HCl(*aq*) | CEM | AEM | NaOH(*aq*) | H_2(*g*) | Pt(*s*)). H_2 gas was sparged into the solution starting at ~2.3 minutes. Pt wires were used as the potential-sensing electrodes.

The *J–E* behavior of a BPM wetted by dilute acid on one side and dilute base on the other side (0.01 M HCl(*aq*)/NaOH(*aq*); Figure 1.7) was similar to that of a BPM wetted by strong acid and strong base. However, the current was about two orders-of-magnitude smaller and the open-circuit potential was about two Nernstian shifts smaller, i.e. ~0.6 V.

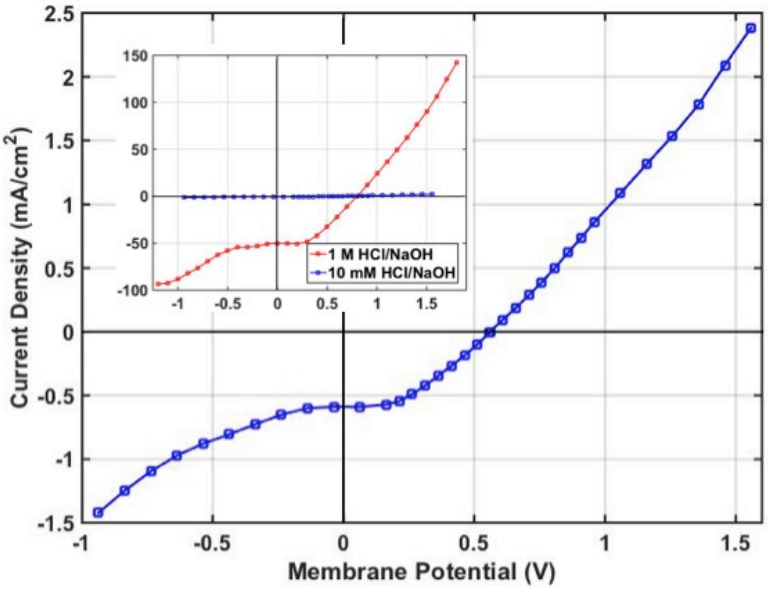

Figure 1.7. *J–E* behavior of a BPM wetted by 0.01 M HCl(*aq*) on the CEM side and 0.01 M NaOH(*aq*) on the AEM side (SCE | HCl(*aq*) | CEM | AEM | NaOH(*aq*) | SCE). Inset: *J–E* behavior of a BPM in 1 M HCl(*aq*)/NaOH(*aq*) (red; same data as in Figure 1.5) and 0.01 M HCl(*aq*)/NaOH(*aq*) (blue; SCE | HCl(*aq*) | CEM | AEM | NaOH(*aq*) | SCE). Both data sets were recorded using SCE potential-sensing electrodes.

The *J–E* behavior of a BPM wetted by 1 M acid/salt or 1 M salt/base (Figure 1.8) resembled that of a BPM wetted by 1 M NaCl (Figure 1.4). An open-circuit potential of ~0 V was measured, and a region of limiting current was observed between 0.0 and 0.8 V and with the BPM passing significantly more current when biased above 0.8 V or below 0.0 V.

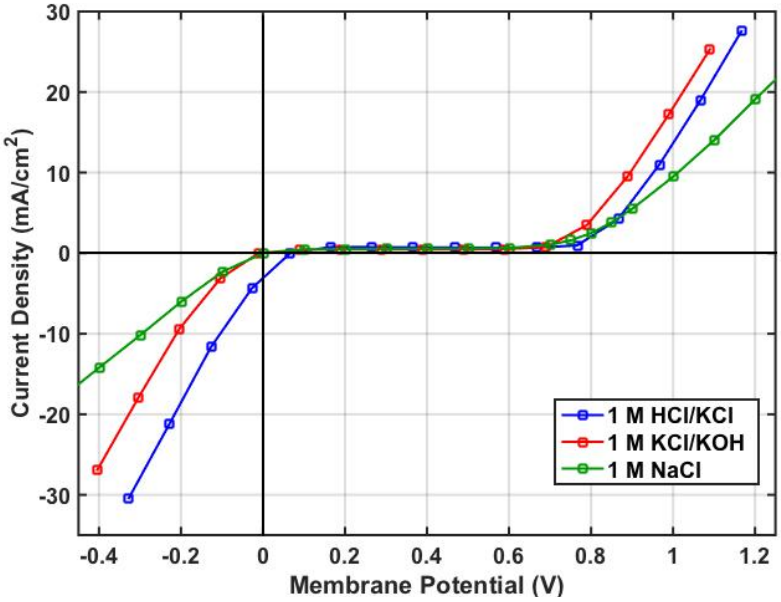

Figure 1.8. *J–E* behavior of a BPM wetted by 1 M aqueous electrolyte solutions: acid/salt (blue; SCE | HCl(*aq*) | CEM | AEM | KCl(*aq*) | SCE), salt/base (red; SCE | KCl(*aq*) | CEM | AEM | KOH(*aq*) | SCE), or salt only (green; same data as in Figure 1.4; SCE | NaCl(*aq*) | CEM | AEM | NaCl(*aq*) | SCE). All data sets were recorded using SCE potential-sensing electrodes.

The *J–E* behavior of a BPM wetted by dilute acid on one side and dilute base on the other side (0.01 M HCl(*aq*)/NaOH(*aq*)) plus 1 M KCl or 1 M NaCl on both sides (Figure 1.9) resembled that of a BPM in 1 M NaCl (Figure 1.4). The open-circuit potential across the BPM in these conditions was ~0 V.

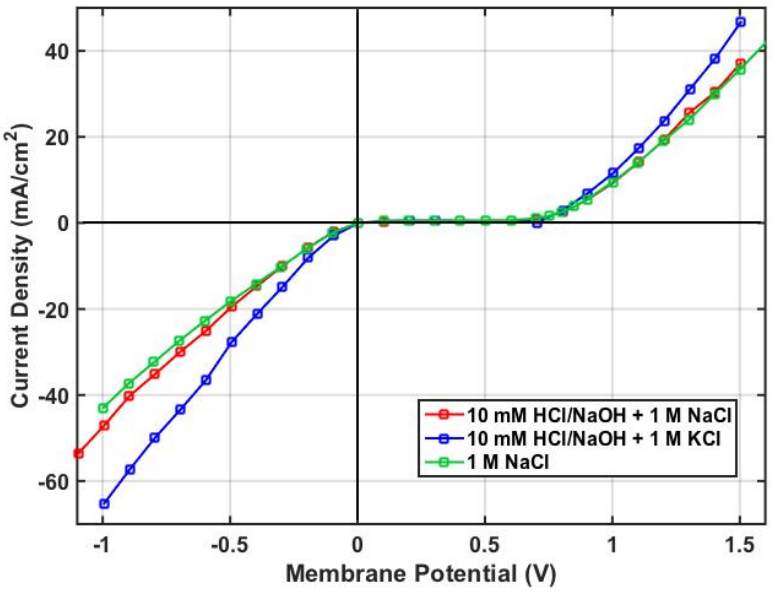

Figure 1.9. *J–E* behavior of a BPM wetted by 0.01 M HCl(*aq*) on the CEM side and 0.01 M NaOH(*aq*) on the AEM side, plus 1 M salt (SCE | HCl(*aq*) + MCl(*aq*) | CEM | AEM | NaOH(*aq*) + MCl(*aq*), where $M^+ = Na^+$ or K^+) or 1 M NaCl(*aq*) only (green; same data as in Figure 1.4; SCE | NaCl(*aq*) | CEM | AEM | NaCl(*aq*)). All data sets were recorded using SCE potential-sensing electrodes.

In order to determine the minimum salt concentration that resulted in a membrane potential of ~0 V, experiments were performed that measured the membrane potential when wetted by dilute acid on one side and dilute base on the other side (0.01 M HCl(*aq*)/NaOH(*aq*)) as a function of the concentration of added salt to both sides (Figure 1.10). The open-circuit membrane potential was found to diminish greatly at an NaCl concentration of ~0.2 M.

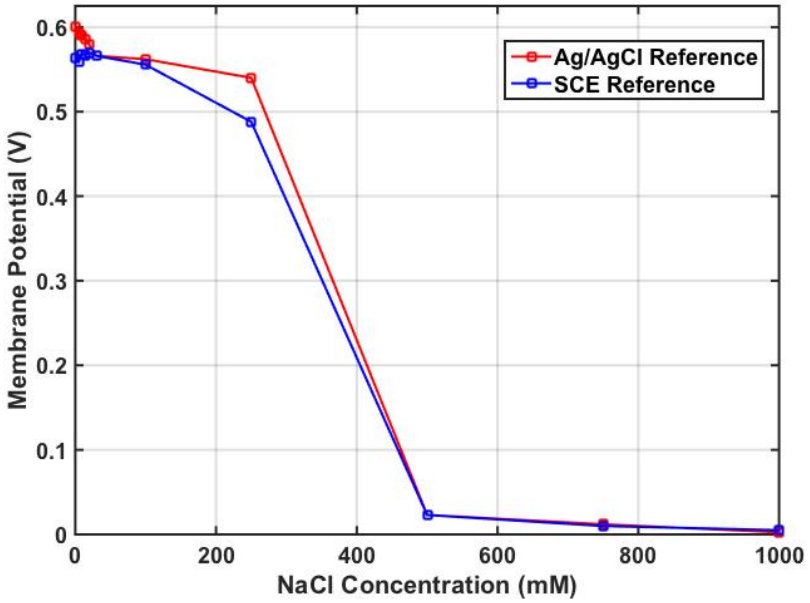

Figure 1.10. Membrane potential of a BPM wetted by 0.01 M HCl(*aq*) on the CEM side and 0.01 M NaOH(*aq*) on the AEM side (Figure 1.5) as a function of the concentration of aqueous NaCl on both sides. Either SCEs or Ag/AgCl wire electrodes were used as the potential-sensing electrodes.

Measurements of the membrane potential as a function of time showed that at a concentration of 0.2 M NaCl, the membrane potential tended toward ~ 0 V over 6 – 10 hours, while at a concentration of 0.1 M NaCl the membrane potential remained at ~530 mV over 7 hours (Figure 1.11).

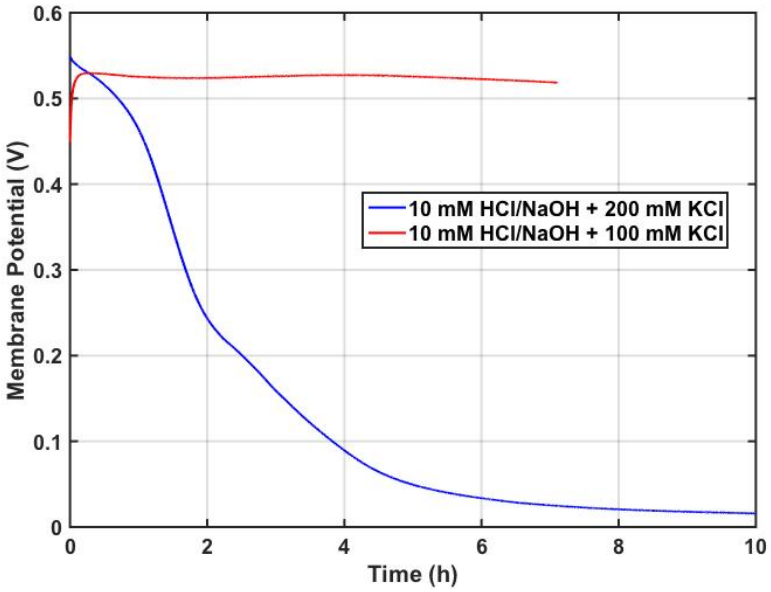

Figure 1.11. Potential across a BPM as a function of time when wetted by aqueous electrolyte consisting of mixed pH conditions plus KCl, as indicated in the figure legend. SCEs were used as the potential-sensing electrodes.

Discussion

Electrochemical behavior of bipolar membranes in 1:1 (M^+X^-) aqueous electrolytes

For systems that exhibit *J–E* behavior similar to that observed in 1 M NaCl(*aq*), reverse-bias results in a small amount current being passed (~0.5 mA/cm^2) due to the large permselectivity of the ion-exchange membranes. This current is a measure of the co-ion "leakiness" of a BPM, and more specifically, the rate of cation transport through the AEM and the rate of anion transport through the CEM. When a membrane potential of ~830 mV is applied, the membrane exhibits what has been termed electric-field enhanced (EFE) water dissociation.[2] The majority of the potential applied to an electrochemical cell with a BPM immersed in 1 M

electrolyte such as NaCl or KCl is present across the space-charge region due to the high resistance of the thin deionized water layer located there. Using Poisson's equation, this suggests that the space-charge region has a very large electric field (up to 10^8 V/m),[2] which increases the unimolecular dissociation rate constant of water, while leaving the bimolecular association rate constant unaffected, leading to a larger concentration of protons and hydroxide ions at equilibrium. This increase in concentration of protons and hydroxide ions is thought to be responsible for the observed breakdown behavior. The protons and hydroxide ions are carried through the appropriate ion exchange layer into the bulk solution.

BPMs function as pseudo-pH meters when wetted by acidic electrolyte on the CEM side and alkaline electrolyte on the AEM side while using reference electrodes that only respond to the generated electric potential (and not the chemical potential of protons or hydroxide ions) (e.g. SCE). When 1 M HCl(*aq*) and 1 M NaOH(*aq*) wet a BPM, the measured open-circuit potential (i.e. electric potential) is ~0.8 V, which is equivalent to 59 mV multiplied by 14 pH units (the difference in pH between 1 M HCl(*aq*) and 1 M NaOH(*aq*)). The magnitude of this potential is expected based on the initial difference in concentration which is maintained by the BPM. The potential forms when protons and hydroxide ions recombine in the space-charge region, thereby leaving uncompensated charges on the fixed groups in the AEM and CEM, which generate an electric potential based Poisson's equation. This recombination process occurs for only a short time and stops once the resulting electric potential difference due to the fixed charge groups is equal and opposite in magnitude to the original chemical potential difference due to the concentration gradient. When the SCE reference electrodes were replaced by quasi-reference electrodes whose potential was sensitive to pH (e.g. Pt wire with H^+/H_2 in solution), both the electric potential and chemical potential should be measured simultaneously. This was thought to

be because $E(H^+/H_2)$, and thus Pt, is sensitive to the chemical potential of protons. This was observed and therefore at equilibrium the membrane potential was ~0 V (Figure 1.6). This is similar to a semiconductor pn-junction where a potential of zero volts is measured at equilibrium, when the chemical potential of electrons and holes is canceled by the electric potential formed in the depletion region.

The *J–E* behavior of BPMs when wetted by more dilute acid and base does not exhibit a limiting current density of 0.5 mA/cm^2 when 0.8 V is applied across the membrane, which is proposed to be due to co-ion leakage which is present in conditions of 1 M NaCl(*aq*). In fact, no limiting current is observed at potentials between 0.6 V (open-circuit potential in 0.01 M HCl(*aq*)/NaOH(*aq*)) and ~0.8 V (potential where significant water dissociation was observed in 1 M NaCl(*aq*)), which we propose is due to the low ionic current being passed through the BPM. We propose that the limiting cathodic current occurs due to limitations in mass transport.

When 1 M or 0.01 M acid and base solutions were separated by a BPM and the potential was measured by SCE reference electrodes, the BPM exhibited an open-circuit potential approximately equal to 59 mV multiplied by the pH difference between the electrolyte solutions (Figure 1.7). However, when a BPM was wetted by an aqueous salt solution on one side and an aqueous acidic electrolyte or aqueous alkaline electrolyte on the other, no open-circuit potential was detected. As shown in Figure 1.8**,** the *J–E* behavior of a BPM in 1 M HCl(*aq*)/KCl(*aq*) or 1 M KCl(*aq*)/KOH(*aq*) appears to mimic that of the BPM in salt only conditions. This arrangement does not follow the Nernstian behavior observed for acid/base conditions. If the BPM behaved similar to that of the 1 M HCl(*aq*)/NaOH(*aq*) experiment, the open-circuit potential would have been approximately equal to 0.4 V, since the pH difference was approximately half of that for the 1 M HCl(*aq*)/NaOH(*aq*) case.

Effects from the addition of salt to cells containing bipolar membranes separating acidic and alkaline aqueous electrolytes

The addition of 1 M salt to both sides of the cell containing 0.01 M HCl(*aq*)/NaOH(*aq*) alters the *J–E* behavior of the BPM so that it resembles that of the BPM in salt only. In this case, the BPM is insensitive to the difference in concentration of protons (hydroxide ions) across the membrane. We believe that this is attributed to the difference in concentration between salt and protons / hydroxide ions in the space-charge region and therefore the effective pH at the interface is closer to 7 than actually observed in the bulk electrolytes. At 0.01 M, the concentration of protons and hydroxide ions are one hundred times smaller than the salt ions. Therefore, salt interacts with the BPM much more frequently than do protons and hydroxide ions, and the Donnan potential due to the protons and hydroxide ions is not present at the interface. A critical concentration where the membrane potential was observed to tend toward ~0 V was determined to occur at a salt concentration of ~0.2 M, which is twenty times the concentration of protons and hydroxide ions (Figure 1.11).

Conclusions

Bipolar membranes can be used to maintain a pH difference between the anolyte and catholyte in electrochemical water splitting technologies. The data herein suggest that the potential measured across the bipolar membrane under conditions of different pH electrolytes is an electric (Donnan) potential that is canceled by the chemical potential of protons when at thermal equilibrium. This hypothesis was corroborated using Pt quasi-reference electrodes whose potentials are sensitive to pH and read ~0 V as the membrane potential. The measured electric potential at SCEs is significantly attenuated when excess salt is present in the electrolyte,

although the pH gradient is still present. This suggests that the electric potential is no longer generated, a hypothesis supported by the idea that the Boltzmann distribution of protons and hydroxide ions in the membranes are overwhelmed by excess salt ions and therefore the driving force for water formation at the junction is small. That is, the effective pH in the space-charge region is sufficiently smaller than in the bulk liquid electrolytes due to significant site occupancy by the ionic salt species.

References

(1) McNaught, A.; Wilkinson, A. IUPAC Gold Book - Donnan exclusion http://goldbook.iupac.org/DT06889.html (accessed Sep 2, 2015).

(2) Mafé, S.; Ramírez, P. *Acta Polym.* **1997**, *48*, 234.

(3) Gaieck, W.; Ardo, S. *Rev. Adv. Sci. Eng.* **2014**, *4*, 1.

(4) Ardo, S.; Park, S. H.; Warren, E. L.; Lewis, N. S. *Energy Environ. Sci.* **2015**, *8*, 1484.

(5) Ünlü, M.; Zhou, J.; Kohl, P. a. *J. Phys. Chem. C* **2009**, *113*, 11416.

(6) McDonald, M. B.; Ardo, S.; Lewis, N. S.; Freund, M. S. *ChemSusChem* **2014**, *7*, 3021.

(7) Vargas-Barbosa, N. M.; Geise, G. M.; Hickner, M. a.; Mallouk, T. E. *ChemSusChem* **2014**, *7*, 3017.

(8) Slade, S.; Campbell, S. a.; Ralph, T. R.; Walsh, F. . *J. Electrochem. Soc.* **2002**, *149*, 1556.

(9) Sze, S. M.; Ng, K. K. In *Physics of Semiconductor Devices, 3rd Edition.; John Wiley & Sons, Inc.; NJ*; 2007; pp 164, 682.

(10) Simons, R. *J. Memb. Sci.* **1993**, *78*, 13.

(11) Fuller, C. S. *Rec. Chem. Prog.* **1956**, *17*, 75.

(12) Lovrecek, B.; Despic, A.; Bockris, J. O. *J. Phys. Chem.* **1959**, *63*, 750.

(13) Bockris, J. O.; Reddy, A. K. N.; Gamboa-Aldeco, M. *Ann. N. Y. Acad. Sci.* **2001**, *1228*, 1.

(14) Balster, J.; Sumbharaju, R.; Srikantharajah, S.; Pünt, I.; Stamatialis, D. F.; Jordan, V.; Wessling, M. *J. Memb. Sci.* **2007**, *287*, 246.

Chapter 2: Dye-Sensitized Ion-Exchange Membranes as Light-Driven Ion Pumps

Introduction

Simple bipolar membranes (BPMs) consist of a cation-exchange membrane (CEM) and an anion-exchange membrane (AEM) joined together in series. When wetted by two different pH electrolyte solutions an electric field is believed to form at the interface of the AEM layer (AEL) and CEM layer (CEL).[1] The electrostatics of this depletion region are similar to those formed by the space-charge region in a semiconductor pn-junction.[2] Motivated by efficient solar cell designs which incorporate a pn-junction that helps separate charge, we aimed to demonstrate a solar cell where the mobile charge carriers were ions instead of electrons and holes. Sensitization to visible light was achieved through incorporation of photoacid dye molecules covalently into a BPM in the space-charge region to convert photon energy into energized charges (i.e. H^+). Illumination of photoacids energizes and liberates protons in the thermally equilibrated excited state because the electron density of the photoacid near a functional group changes significantly.[3] It is proposed that the electric fields within the depletion region will drive photo-liberated protons and hydroxide ions in opposite directions thus generating (ionic) power from sunlight absorption. If the released proton is separated and collected at selective contacts, the current passed through the BPM should increase, while under open-circuit conditions, quasi-electrochemical potentials of protons and hydroxide ions should increase resulting in a change in potential across the membrane. The resulting *J–E* behavior should resemble that of an

illuminated solar cell, where the current-rectifying BPM curve is translated into the power-producing region (second or fourth quadrant).

For initial proof-of-concept studies, Nafion was chosen as the ion-exchange membrane functionalized with photoacids because its properties are very well understood and the Nafion sulfonyl fluoride precursor can be easily functionalized using nucleophilic substitution chemistry. Nafion is a permselective polymer that is primarily composed of a poly(tetrafluoroethylene) backbone with sulfonate groups attached by fluorinated ether linkers, which imparts excellent cationic (protonic) conductivity and chemical and thermal stability (Figure 2.1).

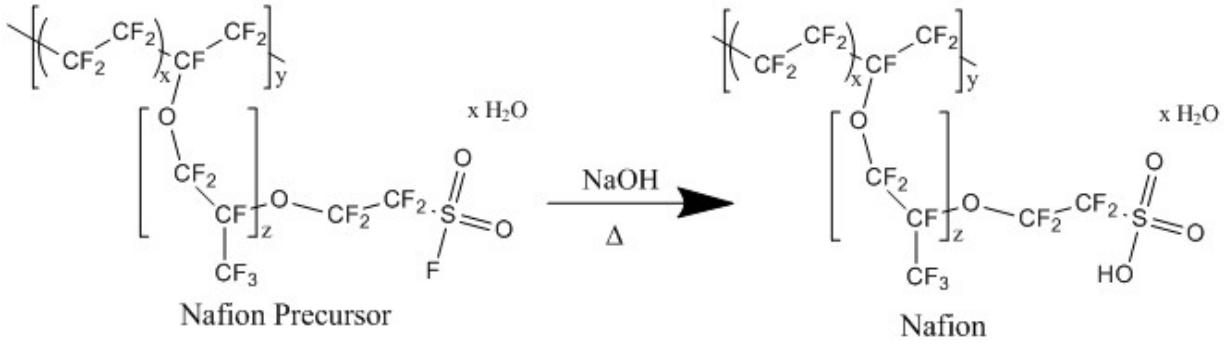

Figure 2.1. Final step in the synthesis of Nafion. The sulfonyl fluoride group is converted to a sulfonate group when treated with sodium hydroxide and heated.

The final step in the synthesis of Nafion is treatment with base to convert the sulfonyl fluoride groups to sulfonate groups via an S_N2 reaction (nucleophilic hydroxyl attack with fluoride as a leaving group; Figure 2.1). Instead, we replaced this step with nucleophilic attack from tris(ethylaminesulfonamide) hydroxypyrene (CS3) to form a sulfonamide (Figure 2.2). CS3 is an analog of a well-known hydroxypyrene photoacid and was synthesized by Christopher Sanborn in the Ardo Group.

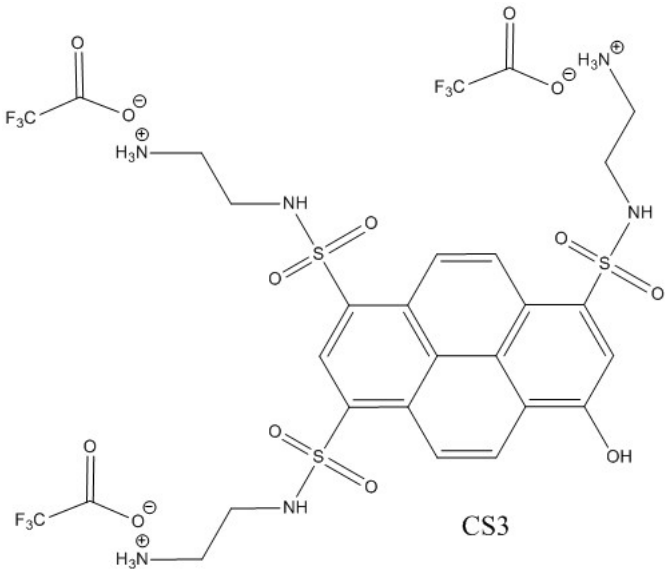

Figure 2.2. Molecular structure of 2,2',2''-((8-hydroxypyrene-1,3,6-trisulfonyl)tris(azanediyl))tris(ethan-1-aminium) 2,2,2-trifluoroacetate (CS3), the photoacid used to functionalize Nafion in this work.

Experimental

Functionalization of Nafion Precursor Films

To functionalize the sulfonyl fluoride groups of the Nafion precursor film with CS3, the film was submerged in isopropyl alcohol containing 3 mg of CS3, 100 molar equivalents of triethylamine, and 25 molar equivalents of NaOH, and heated to 90 °C. Triethylamine and NaOH deprotonated the primary amine groups in CS3 allowing them to perform a nucleophilic attack on the sulfur atom in the sulfonyl fluoride groups (Figure 2.3). The NaOH also converted some of the sulfonyl fluoride groups to sulfonate groups in order to increase the conductivity in the dye-sensitized films. After functionalization, the Nafion–CS3 films were treated with 1 M H_2SO_4 to exchange Na^+ counterions with protons, notably to protonate the hydroxyl group of CS3 so that it could serve as a photoacid.

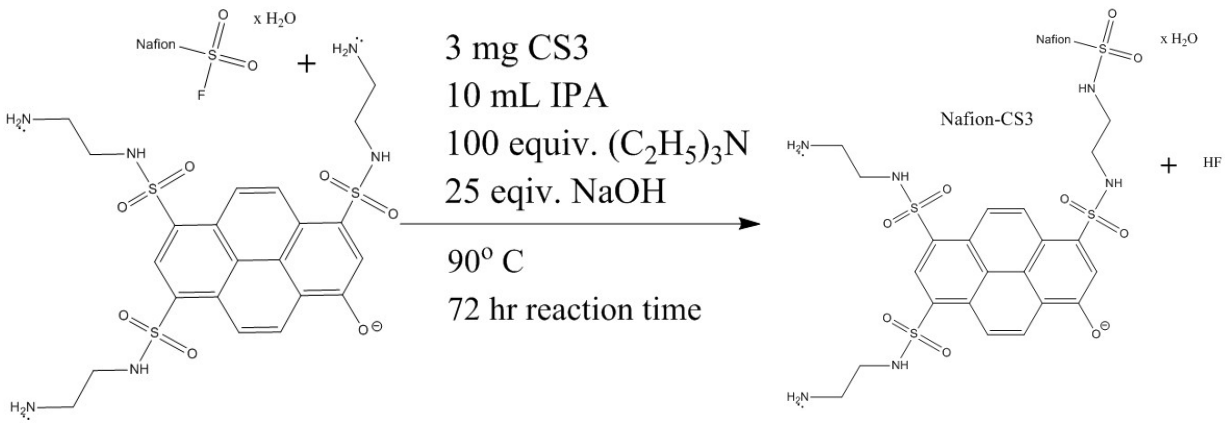

Figure 2.3. Conditions used to functionalize a Nafion precursor membrane with CS3 photoacid molecules.

Determination of the Ion-Exchange Properties of Nafion–CS3

Nafion and Nafion–CS3 films were treated with KCl to exchange the labile protons with K^+. Pieces of Nafion film were then placed in separate vials that contained either anionic (merpacyl orange) or cationic (sevron brilliant red) dyes under stirring. The concentration of the ionic dye solutions was 3 mg per 10 mL. The KCl pretreatment was performed to prevent Nafion from protonating the anionic dyes to neutral species. After 72 hours, the films were analyzed via Ultraviolet–Visible (UV–Vis) spectroscopy to determine the extent of dye absorption into the film.

UV–Vis spectra were taken on an Agilent Cary 60 instrument in transmission mode. The sample holder was removed from the instrument for measurement of membrane samples. Membrane samples were taken from their solutions, rinsed with deionized water, and then placed between two glass slides. The slides were then mounted in front of the detector so that the membrane sample was in the beam path. Spectral resolution was 1 nm and spectra were baselined on a piece of Nafion sandwiched between two glass slides. Accurate measurements did not require use of an integrating sphere because the membranes were transparent.

Dye solution standards were made by adding 30 mg of dye in powder form to 10 mL of deionized water. The resulting solutions were then diluted so that maximum absorbance values were between 0 and 1. UV–Vis measurements of the dye solutions were taken using a plastic cuvette placed in the sample holder and were baselined on deionized water in a plastic cuvette.

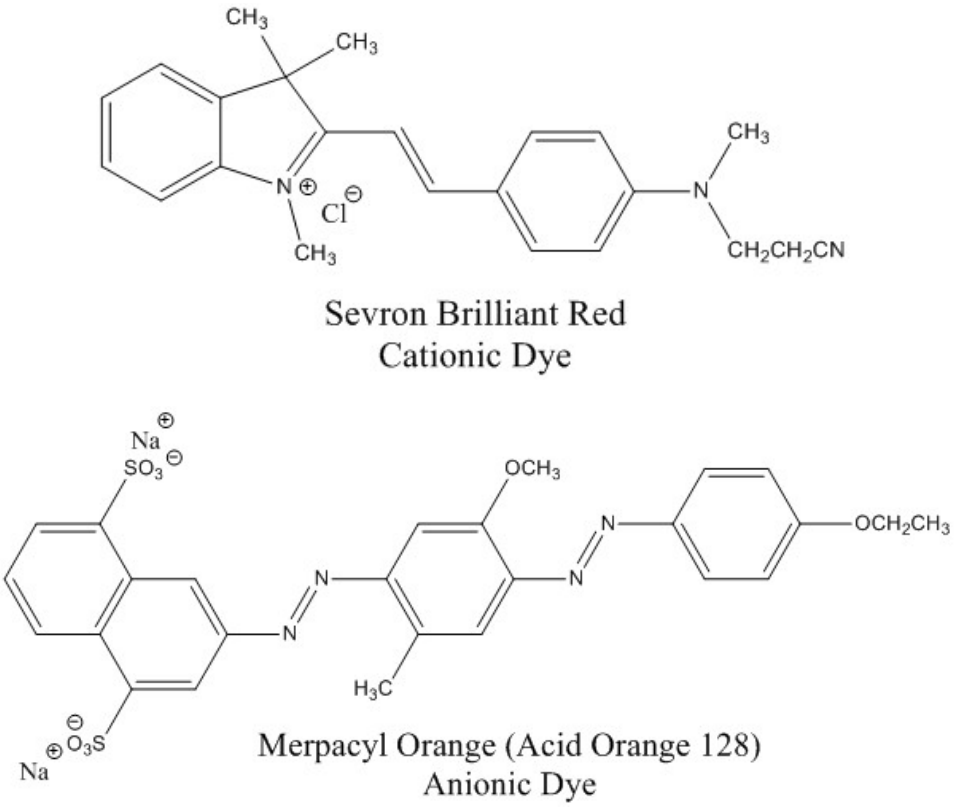

Figure 2.4. Ionic dyes that were employed to determine if photoacid-functionalized Nafion membranes functioned as AEMs and/or CEMs.

Evaluation of Nafion–CS3 Functionalization

In order to support whether the photoacid was covalently or ionically bound to the Nafion surface, two complementary techniques were utilized. First, attempts were made to exchange CS3 with small cations. Functionalized films were soaked in 1 M HCl(*aq*) and 1 M NaCl(*aq*) solutions heated to 75°C for 7 days with stirring. The films were inspected by eye to determine if a significant number of photoacid molecules were exchanged with the aqueous cations.

The films were also analyzed using Fourier-transform infrared (FTIR) spectroscopy to determine if any characteristic peaks of CS3 were present. IR data was obtained with a Jasco FTIR-4700 instrument with an ATR-PRO ONE sample holder. Membrane samples were heated on a hotplate to remove excess water prior to measurement. Samples were placed on the ATR crystal and clamped down with a diamond tip for spectral acquisition. Spectral resolution was 0.5 cm^{-1} and spectra were baselined on air.

Preparation of Nafion–CS3 Membranes

Nafion–CS3 membranes were stored in deionized water when not in use. Prior to performing a measurement, the membrane was removed from its storage container and immediately placed in an electrochemical cell and wetted by the experimental electrolyte solution. After soaking the membrane for 10 min, the electrolyte was discarded and fresh electrolyte was added. This process was repeated one more time.

Preparation of the Electrochemical Cell

The electrochemical cell consisted of two Kel-F (poly(chlorotrifluoroethylene)) blocks each with pre-drilled holes for insertion of the electrodes and a central cylindrical channel for addition of the aqueous electrolyte solution (Figure 2). One side of the cell contained a quartz window for laser light illumination of the functionalized Nafion membranes. Platinum electrodes were fabricated by soldering a 1 cm long 300 μm diameter platinum wire to a piece of insulated tinned Cu wire and sealing the connection with Loctite Hysol 1C two-part epoxy. Unless noted otherwise, these Pt electrodes were used as the power/current-carrying (working and counter) electrodes and were placed on opposite sides of the membrane. The platinum electrodes were

rinsed with deionized water after every electrochemical measurement and stored dry. Standard calomel electrodes (SCEs) were purchased from CH Instruments, Inc. and were used as the reference electrodes, unless noted otherwise. The SCEs were removed from saturated KCl solutions, rinsed with deionized water, and placed in the electrochemical cell. After each electrochemical measurement, the SCEs were rinsed with deionized water and placed in saturated KCl storage solutions.

The electrochemical cell was connected to a BioLogic VSP-300 potentiostat. The current-carrying leads were attached to the platinum electrodes. The platinum electrode on the AEM side of the membrane served as the working electrode, while the platinum electrode on the CEM side of the membrane served as the counter electrode. The main two potential-sensing leads were attached to the SCEs on each side of the membrane so that the potential drop across the membrane could be probed. (In conventional three-electrode electrochemistry experiments, these two leads measure the potential between the working electrode and the reference electrode.) A third (optional) potential-sensing lead was attached to the counter electrode to monitor its potential and help identify anomalous behavior.

Photoelectrochemistry (PEC) Measurements of Nafion–CS3 Membranes

Before starting an electrochemical experiment, an open-circuit potential (E_{oc}) measurement was taken to ensure that the membrane had equilibrated with the electrolyte solutions. After verifying that the membrane potential was stable to within one millivolt for a period of 10 minutes, galvanostatic chronopotentiometry measurements were performed at 0 μA.

Laser excitation was achieved with a < 5 mW output laser pointer attached to a DC power supply that provided a constant potential of 3.0 V. The violet laser wavelength was 405 ± 10 nm

(beam diameter = 1.96 mm; photon flux = 1.16 x 10^{18} photons/s), the green laser wavelength was 532 ± 10 nm (beam diameter = 0.92 mm; photon flux = 7.56 x 10^{18} photons/s), and the red laser wavelength was 650 ± 10 nm (beam diameter = 1.92 mm; photon flux = 8.28 x 10^{18} photons/s). For measurements under illumination, the laser beam was directed through the window in the electrochemical cell so that it illuminated the membrane. The Nafion–CS3 membrane's photo-response was measured by illuminating the membrane with the laser light for a period of 5-10 minutes. The laser was then turned off and the membrane was allowed to equilibrate before the next illumination cycle. All electrodes were positioned out of the beam path.

Laser beam diameters were calculated as the full width at half maximum (FWHM). A silicon diode and digital multimeter were utilized to measure the current response generated by illuminating the diode with the lasers as a function of the distance over which a razor blade blocked the excitation light. The resulting data was fit to a sigmoidal function, and the derivative of this function was taken to obtain the Gaussian beam profile. The width of the Gaussian at half the maximum value was taken to be the diameter of the laser. Refer to Appendix A for Mathematica code used to calculate laser beam diameters. Photon fluxes were calculated using the responsivity of the silicon diode to convert the current generated by the laser into power.

Preparation of Nafion–CS3 BPM

A photoacid-functionalized Nafion membrane was sandwiched between a commercial AEM (AGC Selemion AMV) and commercial CEM (Nafion) to create a bipolar membrane with photoacid molecules in the proposed interfacial space-charge region. The membrane "sandwich" was heated on a hotplate in a humidified atmosphere at 125 °C for 10 minutes to keep the membranes adhered together, albeit weakly.

Photoelectrochemistry (PEC) Measurements of Nafion–CS3 BPM

Before starting an electrochemical experiment, an open-circuit potential (E_{oc}) measurement was taken to ensure that the membrane had equilibrated with the electrolyte solutions. After verifying that the membrane potential was stable to within one millivolt for a period of 10 minutes, potentiostatic chronoamperometry measurements were performed. The *J–E* curve was constructed from a series of these potentiostatic chronoamperometry measurements, where the current at 300 seconds after the start of each potential step – when the value was independent of time – was plotted along with the corresponding potential applied at that step. In order to ensure that the membrane was in good working condition for the entire *J–E* measurement, data points under reverse bias were obtained before those under forward bias where membrane delamination may occur due to excessive water formation at the AEM/CEM interface. Starting at the open-circuit condition, the potential was stepped in increments of +100 mV vs. E_{oc}; this constituted the reverse-bias portion of the *J–E* data where at which time the membrane potential was allowed to equilibrate back to its starting potential. Notably, in neutral-pH salt conditions E_{oc} was zero millivolts initially, and approximately 830 mV after the final reverse-bias chronoamperometry measurement. The forward-bias chronoamperometry data was obtained in the same manner as the reverse-bias data, except that the potential was stepped in increments of –100 mV. After the first "dark" *J–E* curve was constructed, the BPM was allowed to equilibrate and then was illuminated with 405 nm laser light (details provided above) and a "light" *J–E* curve was built. The membrane was then allowed to equilibrate and a final "dark" *J–E* curve was built to assess the properties of the BPM after it had been illuminated.

Current densities were calculated by dividing the current passed through the cell by the geometric area of the membrane exposed to the aqueous electrolyte solution (1.54 cm^2). For all

J–E data, a positive membrane potential corresponds to reverse-bias polarization, and a negative membrane potential corresponds to forward-bias polarization. During reverse-bias polarization, oxidation occurs at the working electrode, which is in contact with the electrolyte that wets the AEM, and reduction occurs at the counter electrode, which is in contact with the electrolyte that wets the CEM.

When evaluating open-circuit membrane potentials over time, the electrodes and extra electrode holes in the electrochemical cell were wrapped with Parafilm to seal off the electrolyte from air and attenuate pH changes due to carbon dioxide dissolution.

Results

Characterization of Functionalized Nafion Membranes

After functionalization of Nafion precursor films with CS3 turned the initially colorless and transparent films into dark red films, which after subsequent treatment with 1 M H_2SO_4, turned the films yellow (Figure 2.5).

Figure 2.5. Digital photograph of a Nafion precursor film (left), Nafion functionalized with CS3 photoacid (middle), and Nafion (right).

In order to determine whether the Nafion-CS3 membrane was a CEM and/or AEM the membranes were soaked in solutions of cationic dyes or anionic dyes and visually inspected and characterized using UV–Vis absorption spectroscopy. Visually, the Nafion–CS3 membranes were observed to absorb the cationic dye to a large extent, and the anionic dye to a minimal extent (Figure 2.6). These findings were corroborated by UV–Vis absorption spectra (Figure 2.7). Control measurements using Nafion only found that cationic dyes absorbed into Nafion well whereas anionic dyes did not (Figure 2.6 and Figure 2.8).

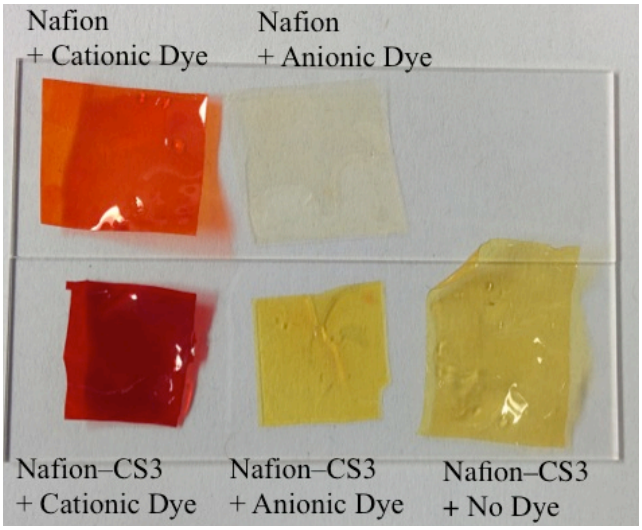

Figure 2.6. Digital photograph of Nafion and Nafion–CS3 membranes that had soaked in solutions of ionic dyes. The cationic dye is red and the anionic dye is orange.

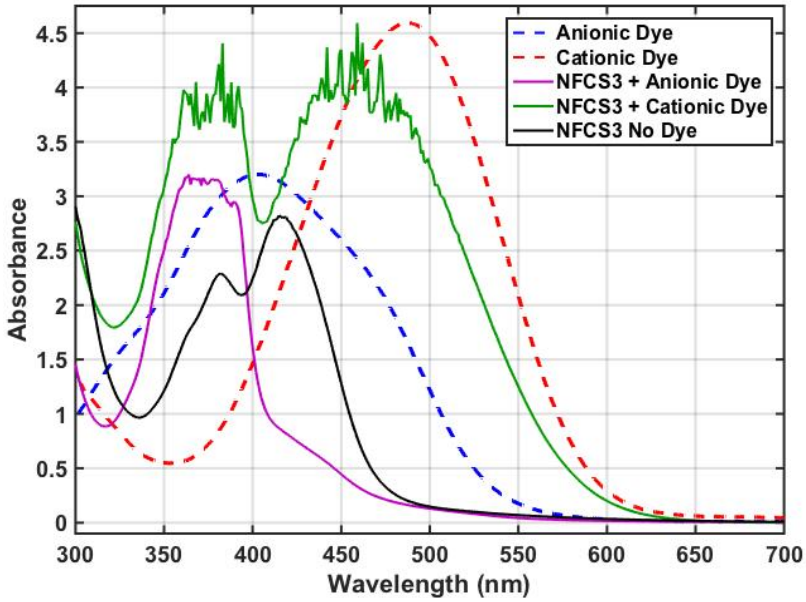

Figure 2.7. UV–Vis spectra of Nafion–CS3 membranes after soaking in a solution of cationic dye (green) or anionic dye (purple), and aqueous solution spectra of the cationic dye (red) and anionic dye (blue). The UV–Vis spectrum of Nafion–CS3 with no dye treatment is sown in black. Dye spectra are normalized to match the maximum absorbance values of the Nafion membrane spectra.

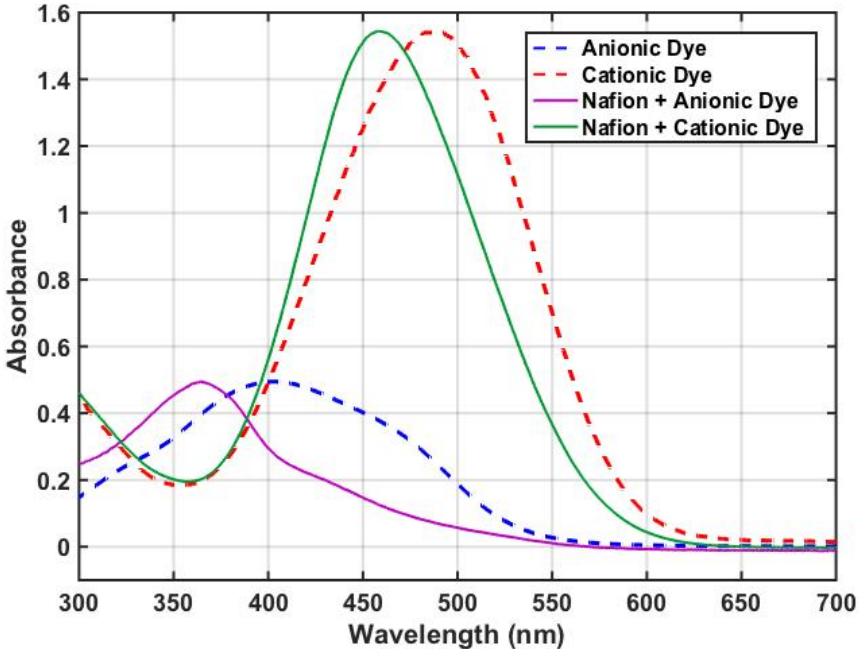

Figure 2.8. UV–Vis spectra of a Nafion membrane after soaking in a solution of cationic dye (green) or anionic dye (purple), and aqueous solution spectra of the cationic dye (red) and anionic dye (blue). Dye spectra are normalized to match the maximum absorbance values of the Nafion membrane spectra.

There was no visual evidence for leaching of photoacid molecules from the membranes when submerged in 1 M salt solutions. IR spectroscopy measurements were performed on the Nafion precursor, Nafion, and Nafion–CS3 films; no peaks from CS3 were observed for the Nafion–CS3 membrane (Figure 2.9). However, spectra for the Nafion–CS3 membrane did exhibit peaks that were present in Nafion (1200-1130 cm^{-1}, C-F bonds). In addition, spectra for the Nafion precursor film had peaks at 800 and 1467 cm^{-1}. These peaks were not present in the Nafion–CS3 spectrum.

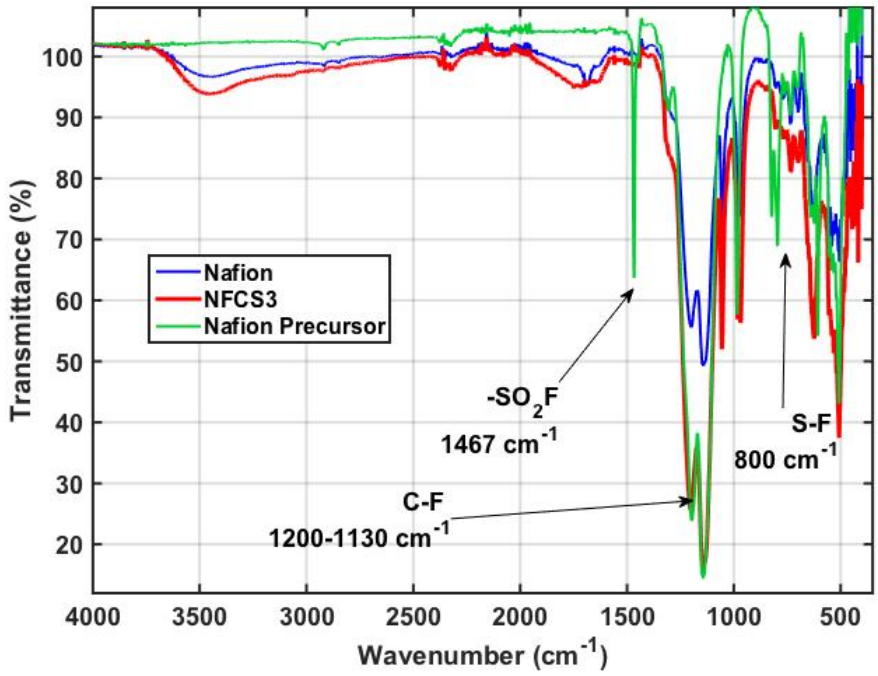

Figure 2.9. FTIR spectra for a Nafion sulfonyl fluoride precursor film (green), a Nafion membrane (blue), and a Nafion–CS3 membrane (red) that did not have NaOH present during functionalization.

Photoelectrochemistry of Nafion–CS3 Membranes and Bipolar Membranes

Photoelectrochemical (PEC) measurements were performed on Nafion–CS3 membranes to determine if they exhibited any noticeable photo-effects. When the membrane was illuminated with purple laser light, fluorescence was observed (Figure 2.10) concomitant with an increase in

the membrane potential. When illuminated with other colors of laser light (i.e. green or red), no fluorescence was observed and the membrane potential did not change (Figure 2.11).

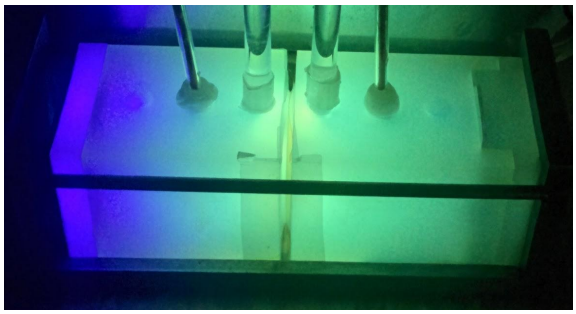

Figure 2.10. Digital photograph of a Nafion–CS3 film fluorescing when illuminated by a violet (405 ± 10 nm) laser. Illumination is incident from the right of the photograph.

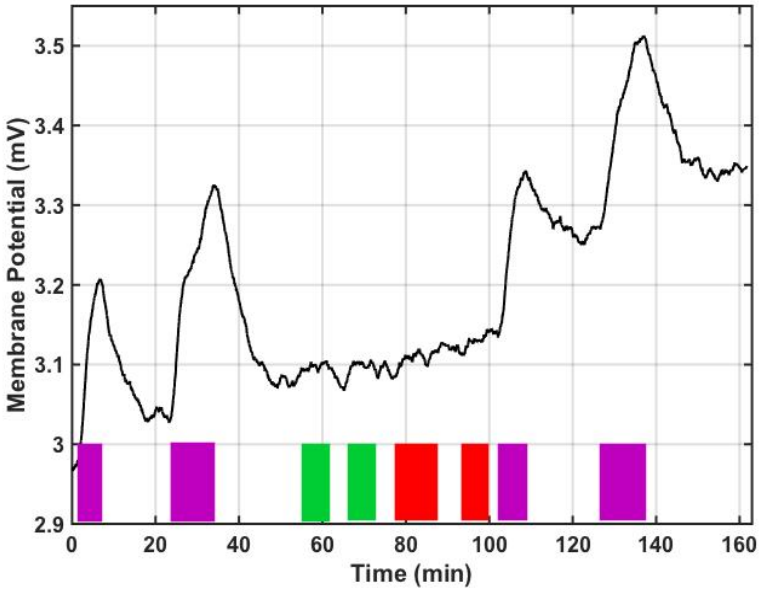

Figure 2.11. Open-circuit voltage measurement over time of Nafion–CS3 immersed in pH 4 (100 µM HCl) + 100 mM KCl and excited with different laser wavelengths. Colored bars are coded to represent the approximate color of laser light used for excitation (violet is 405 nm, green is 532 nm, and red is 650 nm), and their size signifies the time periods over which the membrane was illuminated.

Nafion–CS3 was also characterized photoelectrochemically when sandwiched between a CEM and an AEM as a BPM. The *J–E* behavior of the illuminated photoacid-functionalized BPM was power producing with a non-zero short-circuit photocurrent (19 µA/cm^2) and non-zero open-circuit photovoltage (13 mV). However, the dark post-illumination *J–E* behavior did not

closely match the dark pre-illumination experiment and so the measured magnitude of these effects is imprecise.

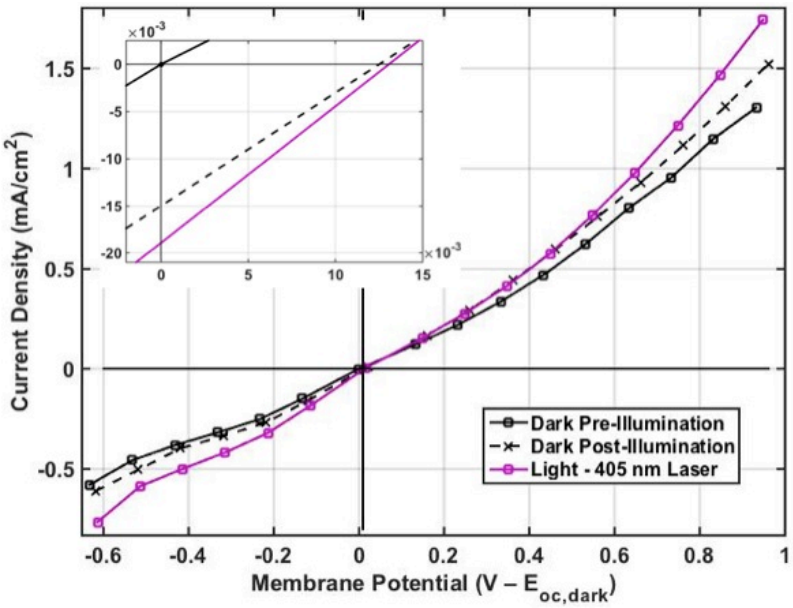

Figure 2.12. (a) *J–E* behavior of Nafion–CS3 sandwiched between a commercial AEM and CEM and wetted by 0.01 M HCl(*aq*) on the CEM side and 0.01 M NaOH(*aq*) on the AEM side (SCE | HCl(*aq*) | CEM | Nafion–CS3 | AEM | NaOH(*aq*) | SCE): dark pre-illumination (solid black), during 405 nm laser light excitation (purple), and dark post-illumination (dotted black). All data sets were recorded using SCE potential-sensing electrodes. All potential values were corrected for the measured open-circuit potential (~0.6 V). Inset: Zoomed-in data on the power-producing region to more clearly show the photovoltage and photocurrent values.

Discussion

Characterization of Functionalized Nafion Membranes

CS3 was used to sensitize Nafion to visible light absorption. This was supported by the fact that Nafion precursor membranes functionalized with CS3 were colored red (not pictured) and CS3 in solution is red. Subsequent treatment with 1 M H_2SO_4 turned the functionalized membrane yellow (Figure 2.5), which is in agreement with the color of protonated CS3 in solution (UV–Vis spectrum in Figure 2.7). This implies that the initial state of the CS3 molecules

in Nafion–CS3 were deprotonated, which is logical because the initial functionalization reaction solution was basic.

The IR spectrum of the Nafion precursor membrane contained peaks at 800 and 1467 cm^{-1}, indicative of S-F and SO_2-F bonds, respectively, while the Nafion–CS3 membrane did not. This suggests that the functionalization process converted most of the sulfonyl fluoride groups present in the Nafion precursor film to covalent sulfonamide bonds with CS3. The membrane used for IR spectral acquisition was only functionalized with CS3; no NaOH was added to the other functionalization reagents. This means that the disappearance of the sulfonyl fluoride functional groups can be attributed to functionalization of the film with CS3 and not a reaction with the sodium hydroxide. However, the lack of IR signal for the sulfonamides implies this is not fully understood. Attempts to ion-exchange CS3 from the membrane were unsuccessful, which supports that CS3 was not ionically bound in the functionalized Nafion films. If CS3 had been ionically bound, soaking the membrane in 1 M aqueous salt solutions would have exchanged some of the CS3 molecules for cations, which would have resulted in coloration of the electrolyte solution.

To determine the ion-exchange groups within a Nafion–CS3 membrane and whether there was a percolation network throughout the membrane, the membranes were soaked with ionic charged dyes. Clearly, cationic dyes absorbed into the membrane while it was less clear whether anionic dyes did (Figures 2.6 and 2.7). Nafion alone was slightly colored by the anionic dyes (Figures 2.6 and 2.8) and thus this suggests that the Nafion-CS3 membrane can primarily act as a CEM. The deep coloration of the film also suggests that a cation-conductive network exists throughout the membrane.

Photoelectrochemistry of Nafion–CS3 Membranes and Bipolar Membranes

In order for Nafion–CS3 to function as a power-producing light-driven ion pump, it must absorb light, separate charge, and collect charge. While absorption spectra suggest that Nafion–CS3 absorbs light, fluorescence observed from a Nafion–CS3 membrane when illuminated with 405 nm light (but not 532 nm light or 650 nm light) was evidence that there is significant radiative decay of the excited-state of CS3 in Nafion. This is important because the ultimate efficiency limit for light-conversion devices occurs when radiative recombination is maximized.[4] Charge separation after optical absorption by 405 nm illumination (but not 532 nm illumination or 650 nm illumination) was indicated by a small measured photovoltage response (Figure 2.11). If no charges had cage escaped from the excited CS3 dyes, then no photovoltage would have resulted. Moreover, the photon fluxes for the red and green lasers were approximately 8 times higher than the violet laser, which further supports that light alone was not the cause of the photo-response.

This Nafion–CS3 membrane was assembled into a bipolar membrane with a CEM on one side and an AEM on the other side to selectively collect the photogenerated charges and hopefully increase the photovoltage response of the membrane. Chronopotentiometry (CP) data taken at open-circuit supported that during laser excitation, the membrane potential increased, presumably due to local pH changes or discharging of the depletion-region capacitance on one side of the membrane due to the aforementioned liberated protons. The increase in potential was an order-of-magnitude larger than observed for Nafion–CS3 alone. Chronoamperometry (CA) data taken at short-circuit showed that under illumination there was an increase in the amount of current passed by the membrane. This increase in current is hypothesized to be due to the

photoacid molecules releasing protons in their excited state, increasing the amount of ions available to conduct current.

The *J–E* behavior for the photoacid-functionalized BPM demonstrates that the device can be used to produce power while under laser illumination. However, the dark post-illumination curve does not show similar *J–E* behavior as the pre-illumination curve. This could be attributed to the fact that during the experiment, the twenty-minute measurement intervals were not sufficiently long enough to allow the membrane to equilibrate back to the pre-illumination conditions. These devices do not respond to illumination at the same rate as solid-state semiconductor devices, and take longer to equilibrate after being illuminated, likely due to an increased resistance and capacitance, and therefore RC time constant for discharging. This hysteretic behavior is indicative of a system that does not quickly reset in the dark to its initial state (i.e. there may be long-lived capacitive effects). This calls into question the magnitude of the produced power, but does not alter the conclusion of light-driven power production.

When constructing the *J–E* curve, reverse polarization is completed before forward polarization, which means that there was a longer temporal gap between the end of the illumination curve and the start of the forward polarization graph compared to the end of the illumination curve and the start of the reverse polarization graph. This had an impact on the *J–E* behavior, as the reverse polarization section of the post-illumination dark curve deviated farther from pre-illumination conditions than the forward polarization dark curve. This indicates that the system needed more time to equilibrate between measurements in order to construct a more accurate *J–E* curve. It is unclear whether it is necessary that the membrane equilibrated under illumination for a longer time prior to recording what was intended to be steady-state data, as only one light cycle was measured.

Conclusions

An artificial light-driven ion pump based on a BPM architecture was reported for the first time. A Nafion precursor membrane was covalently functionalized with photoacid molecules and sandwiched between an AEM and CEM. The resulting membrane exhibited a $V_{oc} \approx 13$ mV and a $j_{sc} \approx 19$ μA/cm^2 under laser light illumination. This model system demonstrated the feasibility of the concept. Materials based on similar chemistries and experimental setups are the focus of ongoing research in the Ardo Group.

References

(1) Mafé, S.; Ramírez, P. *Acta Polym.* **1997**, *48*, 234.

(2) Lovrecek, B.; Despic, A.; Bockris, J. O. *J. Phys. Chem.* **1959**, *63*, 750.

(3) Spry, D. B.; Fayer, M. D. *J. Chem. Phys.* **2008**, *128*, 1.

(4) Shockley, W.; Queisser, H. J. *J. Appl. Phys.* **1961**, *32*, 510.

Appendix A: Mathematica Code for Calculation of Laser Beam Diameter

```
reddata1 = {{0, 0}, {0.05, 0}, {0.1, 0}, {0.15, 0.1}, {0.20, 0.3},
    {0.25, 0.5}, {0.30, 0.7}, {0.35, 0.9}, {0.40, 1}, {0.45, 1.3},
    {0.50, 1.6}, {0.55, 1.9}, {0.6, 2.3}, {0.65, 2.7}, {0.70, 3},
    {0.75, 3.4}, {0.80, 3.8}, {0.85, 4.2}, {0.9, 4.7}, {0.95, 5}, {1, 5.4},
    {1.05, 6}, {1.1, 6.5}, {1.15, 7.2}, {1.20, 7.6}, {1.25, 8.2},
    {1.30, 8.7}, {1.35, 9.3}, {1.40, 9.9}, {1.45, 10.4}, {1.50, 11.3},
    {1.55, 11.9}, {1.6, 12.5}, {1.65, 13.1}, {1.7, 13.7}, {1.75, 14.4},
    {1.80, 15.1}, {1.85, 15.7}, {1.9, 16.4}, {1.95, 17.1}, {2, 17.7},
    {2.05, 18.1}, {2.1, 18.9}, {2.15, 19.6}, {2.20, 20.2}, {2.25, 20.7},
    {2.30, 21.4}, {2.35, 21.9}, {2.40, 22.4}, {2.45, 23}, {2.5, 23.5},
    {2.55, 23.9}, {2.6, 24.3}, {2.65, 24.7}, {2.7, 25}, {2.75, 25.5},
    {2.80, 25.8}, {2.85, 26.1}, {2.9, 26.4}, {2.95, 26.8}, {3, 27.1},
    {3.05, 27.3}, {3.1, 27.5}, {3.15, 27.8}, {3.20, 28.0}, {3.25, 28.3},
    {3.30, 28.5}, {3.35, 28.8}, {3.40, 28.9}, {3.45, 29.1}, {3.5, 29.3},
    {3.55, 29.6}, {3.6, 29.7}, {3.65, 29.9}, {3.7, 30.1}, {3.75, 30.2},
    {3.80, 30.4}, {3.85, 30.6}, {3.9, 30.7}, {3.95, 30.7}, {4.0, 30.7}};
greendata1 = {{0, 0}, {0.05, 0}, {0.1, 0}, {0.15, 0.1}, {0.20, 0.1},
    {0.25, 0.1}, {0.30, 0.1}, {0.35, 0.1}, {0.40, 0.2}, {0.45, 0.2},
    {0.50, 0.2}, {0.55, 0.3}, {0.6, 0.4}, {0.65, 0.5}, {0.70, 0.6},
    {0.75, 0.8}, {0.80, 0.9}, {0.85, 1.1}, {0.9, 1.3}, {0.95, 1.5}, {1, 1.8},
    {1.05, 2}, {1.1, 2.3}, {1.15, 2.6}, {1.20, 3}, {1.25, 3.3}, {1.30, 3.6},
    {1.35, 3.9}, {1.40, 4.1}, {1.45, 4.3}, {1.50, 4.6}, {1.55, 4.8},
    {1.6, 4.9}, {1.65, 5.0}, {1.7, 5.1}, {1.75, 5.2}, {1.80, 5.4}, {1.85, 5.5},
    {1.9, 5.5}, {1.95, 5.6}, {2, 5.7}, {2.05, 5.7}, {2.1, 5.8}, {2.15, 6.0},
    {2.20, 6.0}, {2.25, 6.1}, {2.30, 6.1}, {2.35, 6.1}, {2.40, 6.2},
    {2.45, 6.2}, {2.5, 6.2}, {2.55, 6.3}, {2.6, 6.3}, {2.65, 6.3}, {2.7, 6.4},
    {2.75, 6.4}, {2.80, 6.4}, {2.85, 6.5}, {2.9, 6.5}, {2.95, 6.5}};
violetdata1 = {{0, 0}, {0.05, 0}, {0.1, 0}, {0.15, 0.1}, {0.20, 0.1},
    {0.25, 0.1}, {0.30, 0.2}, {0.35, 0.2}, {0.40, 0.2}, {0.45, 0.3},
    {0.50, 0.3}, {0.55, 0.4}, {0.6, 0.4}, {0.65, 0.4}, {0.70, 0.5}, {0.75, 0.5},
    {0.80, 0.6}, {0.85, 0.6}, {0.9, 0.7}, {0.95, 0.7}, {1, 0.8}, {1.05, 0.8},
    {1.1, 0.9}, {1.15, 0.9}, {1.20, 1}, {1.25, 1}, {1.30, 1.1}, {1.35, 1.1},
    {1.40, 1.2}, {1.45, 1.3}, {1.50, 1.3}, {1.55, 1.4}, {1.6, 1.4},
    {1.65, 1.5}, {1.7, 1.6}, {1.75, 1.6}, {1.80, 1.7}, {1.85, 1.7}, {1.9, 1.8},
    {1.95, 1.9}, {2, 1.9}, {2.05, 2}, {2.1, 2}, {2.15, 2.1}, {2.20, 2.2},
    {2.25, 2.2}, {2.30, 2.3}, {2.35, 2.3}, {2.40, 2.4}, {2.45, 2.4},
    {2.5, 2.5}, {2.55, 2.5}, {2.6, 2.6}, {2.65, 2.6}, {2.7, 2.6}, {2.75, 2.7},
    {2.80, 2.7}, {2.85, 2.7}, {2.9, 2.7}, {2.95, 2.8}, {3.0, 2.8}, {3.05, 2.8}};
model1 = a1 / (1 + b1 * Exp[-c1 (x1 - d1)]) (* equation of
 sigmoidal curve that I want to fit data to *)
ffred1 = FindFit[reddata1, model1, {{a1, 31}, {b1, 7.3}, {c1, 2.3}, {d1, 2.1}},
  x1] (* equation for red laser sigmoidal *)
redplot1 = Show[{ListPlot[reddata1],
   Plot[model1 /. ffred1, {x1, 0, 6}, PlotStyle → {Red}]}, ImageSize → Large]
ffgreen1 = FindFit[greendata1, model1, {{a1, 5}, {b1, 5}, {c1, 3.8}, {d1, 1.7}},
  x1] (* equation for green laser sigmoidal *)
greenplot1 = Show[{ListPlot[greendata1], Plot[model1 /. ffgreen1,
    {x1, 0, 4.5}, PlotStyle → {Green}]}, ImageSize → Large]
ffviolet1 = FindFit[violetdata1, model1,
```

```
  {{a1, 3}, {b1, 5.9}, {c1, 2.33}, {d1, 2}}, x1]
(* equation for violet laser sigmoidal *)
violetplot1 =
 Show[{ListPlot[violetdata1], Plot[model1 /. ffviolet1, {x1, 0, 5.5},
    PlotStyle → {Purple}]}, ImageSize → Large]
```

$$\frac{a1}{1 + b1\, e^{-c1\,(-d1+x1)}}$$

```
{a1 → 30.6438, b1 → 2.13022, c1 → 1.84812, d1 → 1.42845}
```

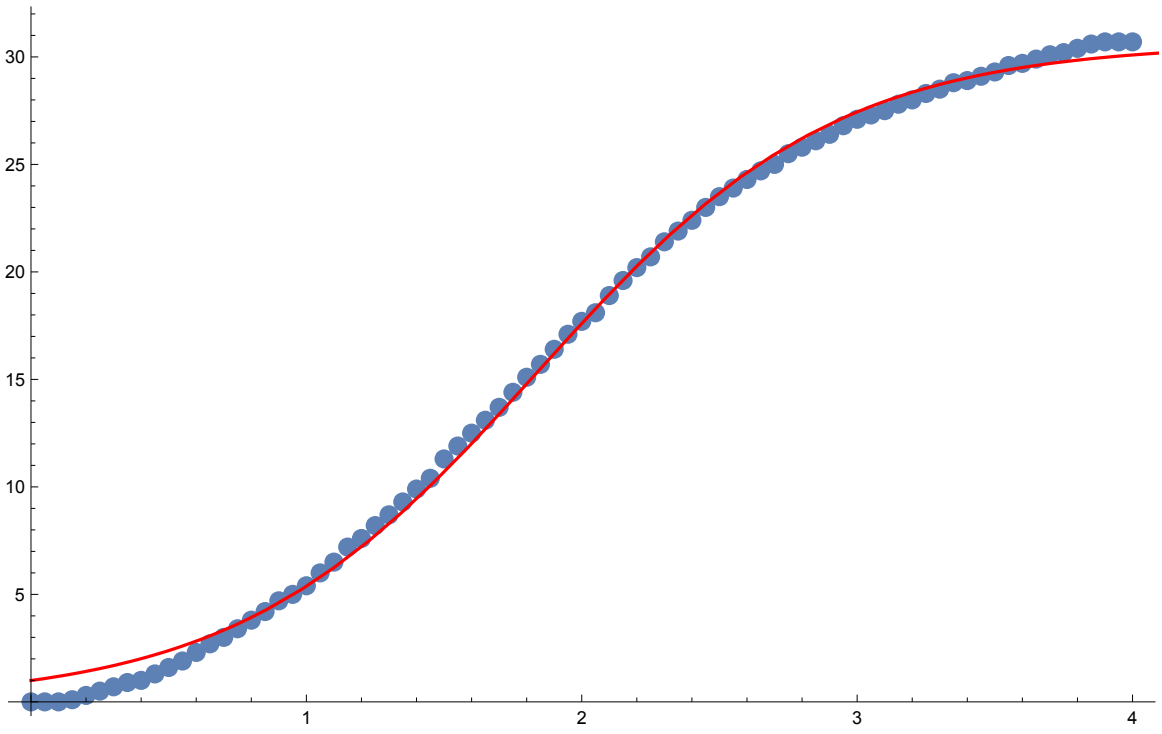


```
{a1 → 6.26978, b1 → 0.763453, c1 → 3.6869, d1 → 1.32431}
```

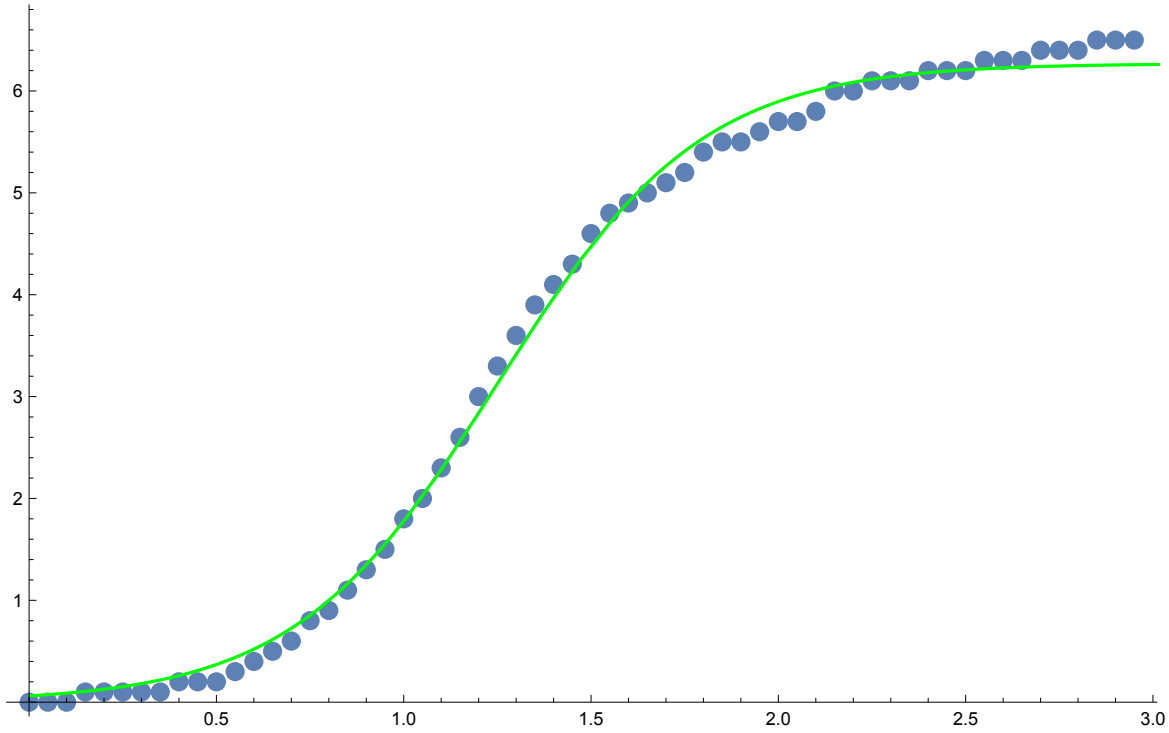

$$\{a1 \to 3.01425,\ b1 \to 1.30056,\ c1 \to 1.79959,\ d1 \to 1.50678\}$$

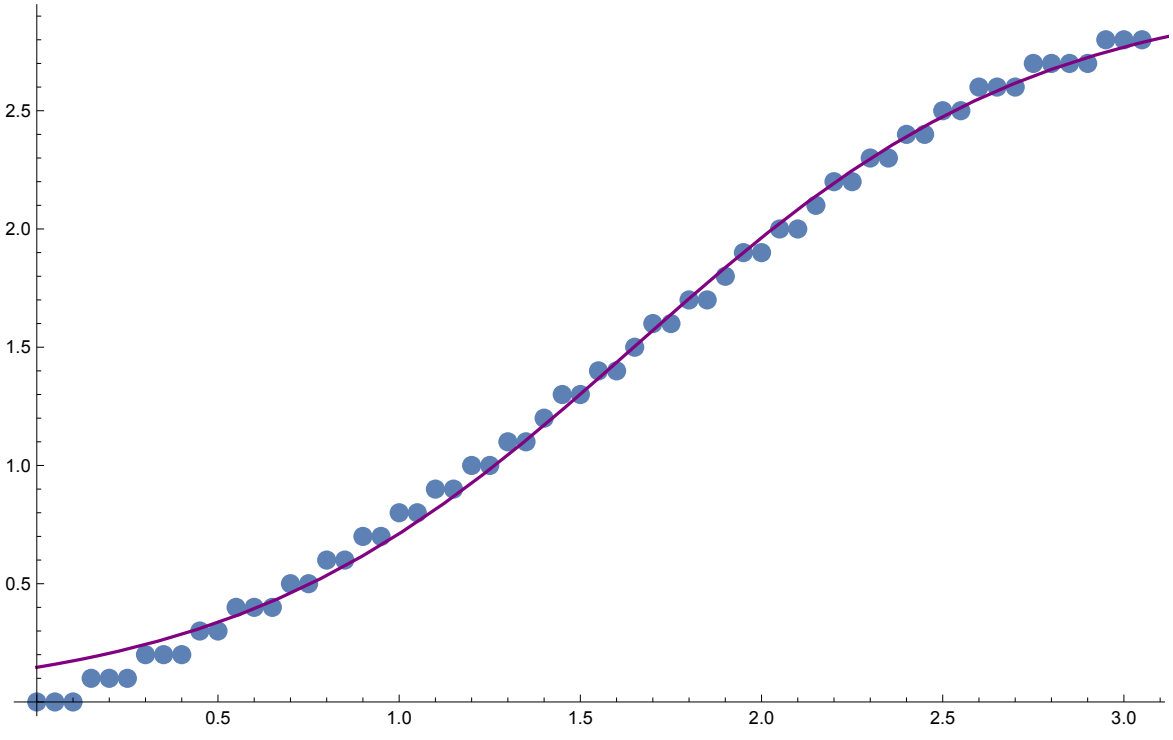

```
(* Plugging in a,b,c,d values to model equation and taking the derivative
 of the sigmoidal to yield the gaussian equations of each laser *)
redgaussian1 = D[model1 /. {a1 → 30.64379840663498`, b1 → 2.1302240706405136`,
      c1 → 1.8481214072981824`, d1 → 1.4284520433063608`}, x1] // FullSimplify
redgaussianplot1 = Plot[redgaussian1, {x1, -2, 6},
  PlotStyle → {Red}, ImageSize → Large]
greengaussian1 =
 D[model1 /. {a1 → 6.269775207179545`, b1 → 0.7634530552379422`,
      c1 → 3.686898170311024`, d1 → 1.3243102926387509`}, x1] // FullSimplify
greengaussianplot1 = Plot[greengaussian1, {x1, -2, 4.5},
  PlotStyle → {Green}, ImageSize → Large]
violetgaussian1 =
 D[model1 /. {a1 → 3.0142545063318624`, b1 → 1.3005647385922758`,
      c1 → 1.799587362002271`, d1 → 1.50677567891696`}, x1] // FullSimplify
violetgaussianplot1 = Plot[violetgaussian1, {x1, -2, 5.5},
  PlotStyle → {Purple}, ImageSize → Large]
```

$$\frac{1690.5\, e^{1.84812\, x1}}{\left(29.8499 + e^{1.84812\, x1}\right)^2}$$

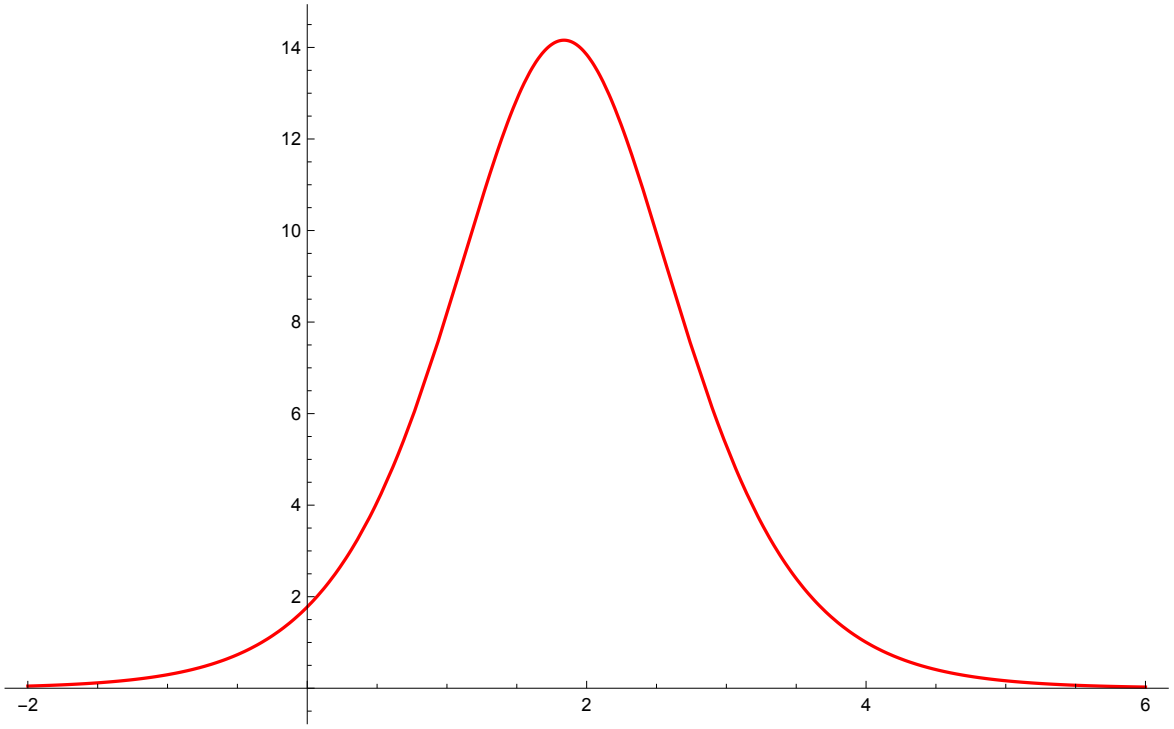

$$\frac{2329.06\, e^{3.6869\, x1}}{\left(100.755 + e^{3.6869\, x1}\right)^2}$$

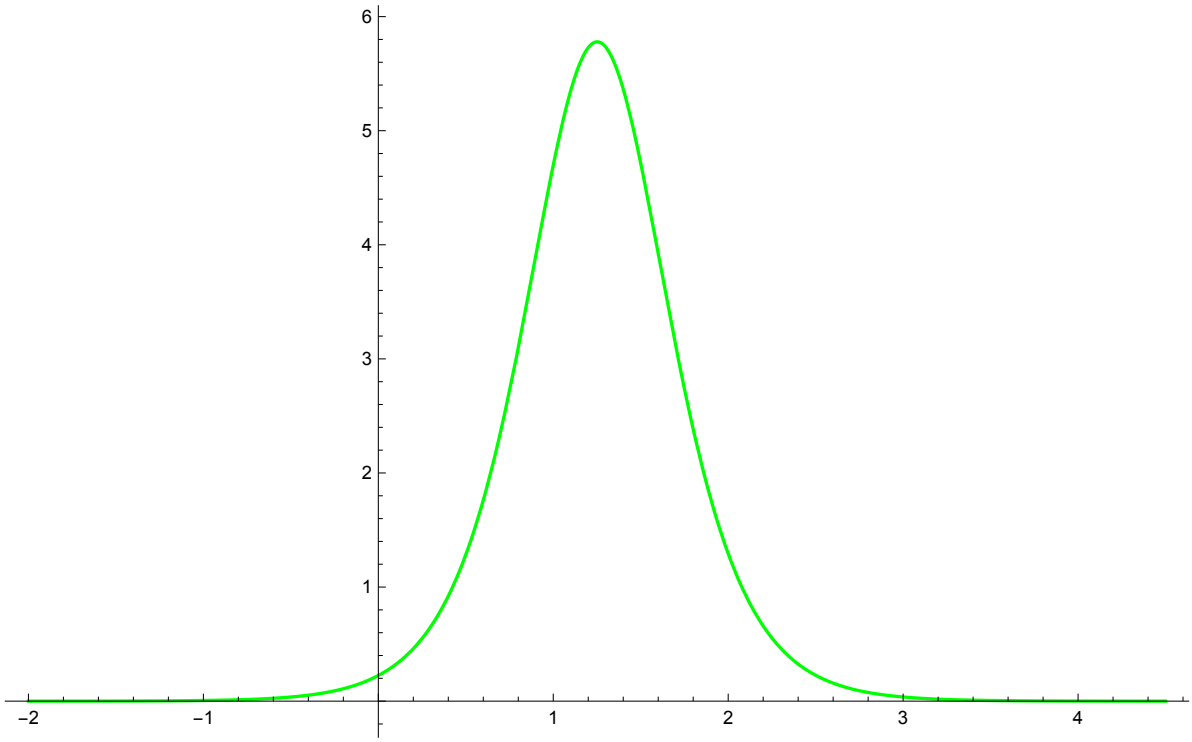

$$\frac{106.196\, e^{1.79959\, x1}}{\left(19.5773 + e^{1.79959\, x1}\right)^2}$$

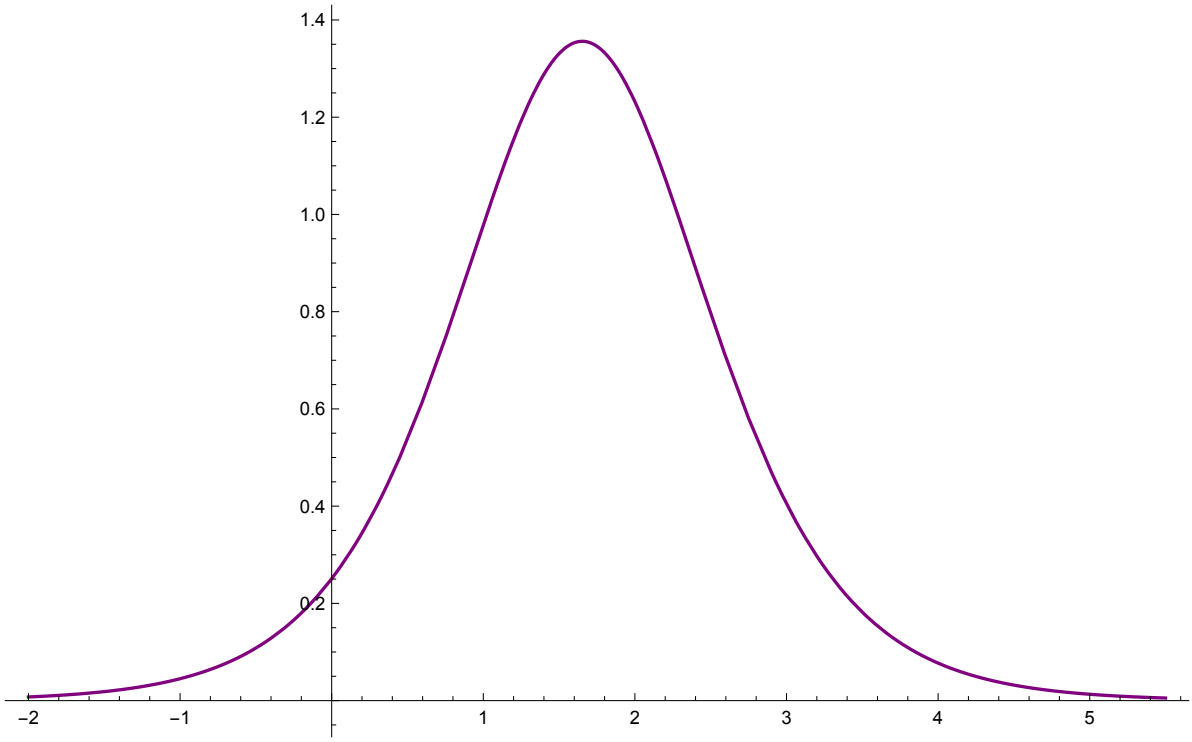

```
(* Taking the derivative of each gaussian equation with respect to x *
dredgaussian1 = D[redgaussian1, x1]
dgreengaussian1 = D[greengaussian1, x1]
dvioletgaussian1 = D[violetgaussian1, x1]
```

$$-\frac{6248.5\, e^{3.69624\, x1}}{\left(29.8499 + e^{1.84812\, x1}\right)^3} + \frac{3124.25\, e^{1.84812\, x1}}{\left(29.8499 + e^{1.84812\, x1}\right)^2}$$

$$-\frac{17174.\, e^{7.3738\, x1}}{\left(100.755 + e^{3.6869\, x1}\right)^3} + \frac{8587.\, e^{3.6869\, x1}}{\left(100.755 + e^{3.6869\, x1}\right)^2}$$

$$-\frac{382.217\, e^{3.59917\, x1}}{\left(19.5773 + e^{1.79959\, x1}\right)^3} + \frac{191.108\, e^{1.79959\, x1}}{\left(19.5773 + e^{1.79959\, x1}\right)^2}$$

```
(* Setting the derivative of each gaussian equal to zero to
 find the x value at which the curve hits a maximum value *)
redxmax1 = Solve[dredgaussian1 == 0, x1] // Flatten
greenxmax1 = Solve[dgreengaussian1 == 0, x1] // Flatten
violetxmax1 = Solve[dvioletgaussian1 == 0, x1] // Flatten
```

Solve::ifun : Inverse functions are being used by Solve, so
some solutions may not be found; use Reduce for complete solution information. >>

$\{x1 \to 1.83764\}$

Solve::ifun : Inverse functions are being used by Solve, so
some solutions may not be found; use Reduce for complete solution information. >>

$\{x1 \to 1.2511\}$

Solve::ifun : Inverse functions are being used by Solve, so
some solutions may not be found; use Reduce for complete solution information. >>

$\{x1 \to 1.65281\}$

```
(* Plugging in the x values found above into the gaussian
 equations to find the maximum y values of each gaussian,
then finding the half maximum values *)
redymax1 = redgaussian1 /. x1 → 1.8376389986037536`
greenymax1 = greengaussian1 /. x1 → 1.2511041366753017`
violetymax1 = violetgaussian1 /. x1 → 1.6528083695145812`
redhalfmax1 = redymax1 / 2
greenhalfmax1 = greenymax1 / 2
violethalfmax1 = violetymax1 / 2
```

```
14.1584
```

```
5.77901
```

```
1.3561
```

```
7.07918
```

```
2.8895
```

```
0.678052
```

```
(* Plugging in the half maximum y values found
 above to find the two x values on the gaussian curve *)
Solve[redgaussian1 == redhalfmax1, x1]
Solve[greengaussian1 == greenhalfmax1, x1]
Solve[violetgaussian1 == violethalfmax1, x1]
```

Solve::ratnz : Solve was unable to solve the system with inexact coefficients. The answer was obtained by solving a corresponding exact system and numericizing the result. ≫

```
{{x1 → ConditionalExpression[
     0.54109 (1.63343 + (0. + 6.28319 i) C[1]), C[1] ∈ Integers]},
 {x1 → ConditionalExpression[0.54109 (5.15893 + (0. + 6.28319 i) C[1]),
     C[1] ∈ Integers]}}
```

Solve::ratnz : Solve was unable to solve the system with inexact coefficients. The answer was obtained by solving a corresponding exact system and numericizing the result. ≫

```
{{x1 → ConditionalExpression[
     0.271231 (2.84995 + (0. + 6.28319 i) C[1]), C[1] ∈ Integers]},
 {x1 → ConditionalExpression[0.271231 (6.37544 + (0. + 6.28319 i) C[1]),
     C[1] ∈ Integers]}}
```

Solve::ratnz : Solve was unable to solve the system with inexact coefficients. The answer was obtained by solving a corresponding exact system and numericizing the result. ≫

```
{{x1 → ConditionalExpression[
     0.555683 (1.21163 + (0. + 6.28319 i) C[1]), C[1] ∈ Integers]},
 {x1 → ConditionalExpression[0.555683 (4.73712 + (0. + 6.28319 i) C[1]),
     C[1] ∈ Integers]}}
```

```
(* Taking the two x values and subtracting
 them to find the laser beam diameter *)
reddiameter1 = 0.5410899933581347` *
  (5.1589271462458886` - 1.6334327981652943`)
greendiameter1 = 0.2712307077132105` *
  (6.375440726498049` - 2.8499463782553973`)
violetdiameter1 = 0.5556829421647927` *
  (4.7371202276321505` - 1.2116258795478898`)
```

```
1.90761
```

```
0.956222
```

```
1.95906
```

```
(* Experiment results: Red = 1.90761mm,
Green = 0.956222mm, Violet = 1.95905mm *)
```